frontiers in Earth Science

BRIEF RESEARCH REPORT
published: 17 June 2021
doi: 10.3389/feart.2021.579198

Sinking Diatom Assemblages as a Key Driver for Deep Carbon and Silicon Export in the Scotia Sea (Southern Ocean)

D. Zúñiga[1,2,3], A. Sanchez-Vidal[4], M. M. Flexas[5], D. Carroll[6], M. M. Rufino[2,7], G. Spreen[8], A. Calafat[4] and F. Abrantes[2,3]*

[1]Instituto de Investigacións Mariñas, Spanish National Research Council (CSIC), Vigo, Spain, [2]Div. Geologia e Georecursos Marinhos, Portuguese Institute for the Sea and Atmosphere (IPMA), Lisbon, Portugal, [3]CCMAR - Centre of Marine Sciences, University of Algarve, Faro, Portugal, [4]GRC Geociències Marines, Universitat de Barcelona, Barcelona, Spain, [5]California Institute of Technology, Pasadena, CA, United States, [6]Moss Landing Marine Laboratories, San José State University, Moss Landing, CA, United States, [7]CEAUL, Centre of Statistics and its Applications, Faculty of Sciences, University of Lisbon, Lisbon, Portugal, [8]Institute of Environmental Physics, University of Bremen, Bremen, Germany

OPEN ACCESS

Edited by:
Maureen H Conte, Bermuda Institute of Ocean Sciences, Bermuda

Reviewed by:
Ian Salter, Alfred Wegener Institute Helmholtz Centre for Polar and Marine Research (AWI), Germany
Tom Trull, Commonwealth Scientific and Industrial Research Organisation (CSIRO), Australia

***Correspondence:**
D. Zúñiga
imissons@gmail.com

Specialty section:
This article was submitted to Biogeoscience, a section of the journal Frontiers in Earth Science

Received: *01 July 2020*
Accepted: *26 May 2021*
Published: *17 June 2021*

Citation:
Zúñiga D, Sanchez-Vidal A, Flexas MM, Carroll D, Rufino MM, Spreen G, Calafat A and Abrantes F (2021) Sinking Diatom Assemblages as a Key Driver for Deep Carbon and Silicon Export in the Scotia Sea (Southern Ocean). Front. Earth Sci. 9:579198. doi: 10.3389/feart.2021.579198

Physical and biogeochemical processes in the Southern Ocean are fundamental for modulating global climate. In this context, a process-based understanding of how Antarctic diatoms control primary production and carbon export, and hence global-ocean carbon sequestration, has been identified as a scientific priority. Here we use novel sediment trap observations in combination with a data-assimilative ocean biogeochemistry model (ECCO-Darwin) to understand how environmental conditions trigger diatom ecology in the iron-fertilized southern Scotia Sea. We unravel the role of diatoms assemblage in controlling the biogeochemistry of sinking material escaping from the euphotic zone, and discuss the link between changes in upper-ocean environmental conditions and the composition of settling material exported from the surface to 1,000 m depth from March 2012 to January 2013. The combined analysis of *in situ* observations and model simulation suggests that an anomalous sea-ice episode in early summer 2012–2013 favored (*via* restratification due to sea-ice melt) an early massive bloom of *Corethron pennatum* that rapidly sank to depth. This event drove high biogenic silicon to organic carbon export ratios, while modulating the carbon and nitrogen isotopic signals of sinking organic matter reaching the deep ocean. Our findings highlight the role of diatom ecology in modulating silicon vs. carbon sequestration efficiency, a critical factor for determining the stoichiometric relationship of limiting nutrients in the Southern Ocean.

Keywords: diatoms, sea ice, marginal ice zone, carbon export, biogenic silicon, scotia sea, southern ocean, corethron pennatum

INTRODUCTION

The Southern Ocean (SO) is one of the most productive regions in the global ocean, and through its connection with all other basins, has sparked intense debate of how this remote region modulates global climate (Falkowski et al., 1998; Sarmiento et al., 2004). In this context, phytoplankton are of utmost importance due to their critical role in ocean carbon sequestration. These tiny organisms are fundamental for modulating climate change through their capacity to consume and export

atmospheric carbon dioxide (CO_2) to bottom sediments (Smetacek et al., 2012; Boyd et al., 2016; Tréguer et al., 2017). Furthermore, phytoplankton in the SO may influence productivity at global scales by modifying the stoichiometric relationships of SO nutrients that are transported to distant regions around the global ocean (Pondaven et al., 2000; Ragueneau et al., 2000; Brzezinski et al., 2002; Matsumoto and SarmientoBrzezinski, 2002).

While the phytoplankton community varies between different SO biogeochemical provinces, there is clear consensus that diatoms, which are unicellular organisms with silica skeletons, are the dominant phytoplankton group during elevated primary productivity events (Bathmann et al., 1997; Arrigo et al., 1999; Landry et al., 2002). In the remote SO, where macronutrients remain high, dissolved iron (dFe) content in combination with light availability acts as the limiting factor for diatom growth (Martin et al., 1990; Buma et al., 1991; Boyd et al., 2007). Furthermore, dFe variability can also shift diatoms community structure, through the promotion of different physiological and survival strategies (Hutchins and Bruland, 1998; Takeda, 1998; Marchetti and Cassar, 2009; Quéguiner, 2013). The largest ecological manipulation experiment to date in the SO revealed that Fe addition promoted thin-shelled small diatoms, while Fe-limited conditions led to the dominance of heavily-silicified diatoms (Assmy et al., 2013). While the results from this groundbreaking experiment provide invaluable information linking diatom ecology to SO biogeochemistry, other critical aspects, such as how other environmental factors (e.g., irradiance, temperature, and water column stability) control the diatom species succession remain poorly understood (Boyd, 2013).

Due to their high sinking rates, diatoms have the capacity to transfer organic carbon (OC) and biogenic silicon (bioSi) from the productive surface layer to the deep ocean. As a result, diatoms are widely identified as the most relevant phytoplankton group for unraveling SO organic carbon cycling (Bathmann et al., 1991; Smetacek et al., 2012; Krause and Lomas, 2020). To fully understand diatom-driven export, and hence how carbon and silicon are sequestered, it is also critical to consider diatom ecological traits. These traits respond to favorable growth conditions, determine the survival of one species vs. another, and consequently impacts settling velocity. While sinking, the intact survival of diatom frustules depends on the resistance of their siliceous skeletons to dissolution and the impact of remineralization processes on their cell's organic content. These two aspects, along with the capability of diatoms to avoid grazing by pelagic zooplankton, must be considered for a complete understanding of which diatom species reach the seafloor and impact sediment composition. In this context, studies based on sediment trap data are especially important, since they represent the missing link between processes occurring at the ocean surface and the seafloor. Despite sparse sediment trap observations in the SO, previous *in-situ* studies have been fundamental for understanding the role of seasonal diatom assemblages in determining the transfer efficiency of biogenic matter escaping the epipelagic domain (Fischer et al., 2002; Pilskaln et al., 2004; Salter et al., 2007; Ichinomiya et al., 2008; Salter et al., 2012; Grigorov et al., 2014; Rembauville et al., 2015; Rigual-Hernández et al., 2015, 2016; Rigual-Hernandez et al., 2019). However, only few studies discuss variability in export rates by considering environmental factors to regulate seasonal diatom production in the upper water column (Salter et al., 2012; Rigual-Hernández et al., 2015, 2019; Rembauville et al., 2018).

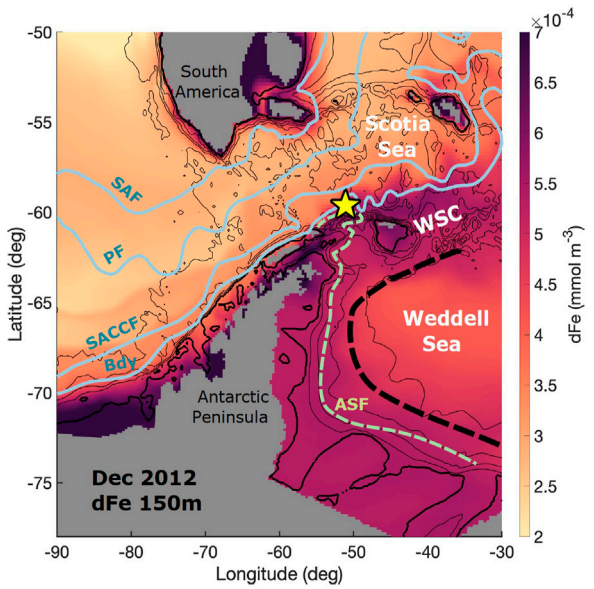

FIGURE 1 | Map of the study region depicting bathymetry, main oceanographic fronts and the sediment trap location (yellow star). ECCO-Darwin dissolved iron concentration (dFe, in color) for the month of December 2012 at 150 m depth shows the supply of dFe from the tip of the Antarctic Peninsula. Antarctic Circumpolar fronts (Orsi et al., 1995) are shown in gray (SAF: Sub-Antarctic front; PF: Polar Front; SACCF: Southern Antarctic Circumpolar Current Front; Bdy: Southern boundary of the Antarctic Circumpolar Current); the Antarctic Slope Front (ASF) is shown in light green; and the outer limit of the Weddell Gyre is indicated with a dashed black line. The zonal band between the southern boundary (Bdy) of the ACC and the northern limit of the Weddell Gyre is known as the Weddell Scotia Confluence (WSC; Patterson and Sievers, 1980). Isobaths are shown as black contours (500 m, thick line; every 1,000 m, thin lines).

In the South Atlantic sector of the SO, naturally Fe-enriched shelf waters from the Antarctic Peninsula meet the southern boundary of the Antarctic Circumpolar Current (**Figure 1**) (Orsi et al., 1995; Dulaiova et al., 2009; DeJong et al., 2012; Jiang et al., 2019; Sanchez et al., 2019). This leads to relatively high rates of primary production compared to other SO biogeochemical regions (de Baar et al., 1995; Holm-Hansen et al., 2004; Ardelan et al., 2010). Despite their importance in terms of quantifying productivity, previous particle flux studies in this region are scarce and are based on free-drifting traps deployed for short time periods (Bodungen et al., 1986; Gersonde and Wefer, 1987; Abelmann and Gersonde, 1991; Leventer, 1991), which limits our understanding of carbon and silicon sequestration on seasonal and longer timescales.

The primary goal of this study is to determine the role of diatoms in driving the export of OC and bioSi to depth in the Fe-fertilized southern Scotia Sea by analyzing sinking diatom

assemblage, along with isotopic and major element composition of settling particles. These data provide unprecedented detail on: 1) how diatom survival strategies regulate the biogeochemical signature of exported particles and 2) how diatom floristics respond to changing environmental conditions. Our work fills a critical gap in understanding the role of diatom ecology in the SO carbon cycle, while providing novel information on the use of fossil diatom assemblages as a proxy for past primary production. Ultimately, our results provide new insight on the role of diatoms in the biogeochemistry cycle of SO waters.

DATA AND METHODS

Study Region

The study site is located in the Weddell-Scotia Confluence (WSC, **Figure 1**), a weakly-stratified region with sub-surface temperature and salinity that is lower than waters located to the north and the south (Patterson and Sievers, 1980; Orsi et al., 1993; Whitworth et al., 1994). Relatively warm sub-surface waters in the north (Circumpolar Deep Water, in the Scotia Sea) and the south (Warm Deep Water, in the Weddell Sea) mark the meridional extension of the Confluence Zone. The currents associated with these water masses (the Antarctic Circumpolar Current and the Weddell Gyre) confer a general eastward zonal flow on both limits. The weak stratification of the WSC is caused by strong lateral mixing along isopycnals (Whitworth et al., 1994), and enhanced diapycnal mixing near the bottom (Naveira-Garabato et al., 2002). Rectified tidal flows are responsible for sustaining the Antarctic Slope Front (Jacobs, 1991) over the complex double-ridge topography (Heywood et al., 2004; Flexas et al., 2015). Wind forcing controls the surface circulation over the South Scotia Ridge. In particular, wind stress curl over the Weddell Gyre determines the pathway of surface waters exported into the Scotia Sea (Youngs et al., 2015) and thus has a large impact on surface-ocean chlorophyll patterns in this region (Thompson and Youngs, 2013). Sea ice from the continental shelf and slope of the Weddell Sea is advected by local winds, which also control sea-ice concentration trends (Holland and Kwok, 2012) (**Supplementary Figure S1**).

Sediment Trap Observations

In the framework of a multi-year international program focused on studying the Antarctic Slope Front over the South Scotia Ridge (Palmer et al., 2012; Flexas et al., 2015), an instrumented mooring with a near-bottom sediment trap (1,000 m depth) was deployed from March 2012 toJanuary 2013 at the northern slope of the South Scotia Ridge (60°S, 53°W; 1,130 m isobath) with sampling periods of one month. Representing dates are referred to the middle point of each sampling period that begins the first day of the corresponding month. The sediment trap was a Technicap PPS3 (0.125 m^2 collecting area) with a cylindroconical collection funnel and 12 polypropylene collecting cups, which were set to rotate every month. Before the deployment, the cups were cleaned with 0.5 N HCl, rinsed with ultrapure water, and filled with buffered 5% (v/v) formaldehyde solution in 0.45 μm filtered seawater. After recovery, the closed cups were stored in the dark at 2–4°C until they were processed in the laboratory, within a maximum delay of a few weeks. After decantation of the supernatant, particles were wet-sieved through a 1 mm nylon mesh to retain the largest swimmers, while the smaller ones were removed under a dissecting microscope using fine tweezers. The sample was then divided into 6–12 equal wet aliquots for biogeochemical analyses and diatom identification using a rotary splitting method following the methodology described in Heussner et al. (1990).

The total mass was determined gravimetrically on two or three sub-samples. The replicates were filtered onto cellulose acetate membranes (0.45 μm pore size, 47 mm diameter), rinsed with distilled water to remove salts and excess formalin, and dried to constant weight at 40 C during 24 h. One of the aliquots of each sediment trap sample was freeze-dried, ground and homogenized. Assuming that all the inorganic carbon was constituted by calcium carbonate, the organic matter (organic carbon × 2) and the calcium carbonate [(total carbon–organic carbon) × 8.33] were calculated. The lithogenic (terrigenous) fraction was obtained by the difference between the total mass and the sum of the biogenic compounds [organic matter, calcium carbonate and biogenic silicon (bioSi)].

Total and organic carbon (OC) and total nitrogen (TN) contents, and the stable isotope composition of OC and TN, were measured on an elemental analyzer interfaced to an isotope ratio mass spectrometer at the Scientific and Technological Centers of the University of Barcelona. Samples for OC analysis were first treated with HCl 25% to remove inorganic carbon. The results of isotopic analyses are presented in the conventional δ notation, which is defined as $\delta X = [(Rsample/Rstandard)- 1] \times 1{,}000$, where X is ^{13}C or ^{15}N and R is the isotopic ratio of $^{13}C/^{12}C$ or $^{15}N/^{14}N$. Isotopic ratios of the samples (Rsample) are expressed relative to those of a standard (Rstandard), the Pee Dee Belemnite for C and atmospheric N_2 for N.

BioSi was analyzed using a two-step extraction with 0.5 M Na_2CO_3 (2.5 h each) separated after filtration of the leachate. Inductive Coupled Plasma Atomic Emission Spectroscopy (ICP-AES) was used to analyze Si and Al contents in the leachates, and a correction of the Si of the first leachate by the Si/Al relation of the second leachate was applied in order to correct for the excess Si dissolved from aluminosilicates and obtain the bioSi concentration (Kamatani and Oku, 2000). Thus, in this paper we provide bioSi (silicon) strictly speaking, not silica (SiO_2) neither amorphous hydrated silica (opal, SiO_2 $0.4H_2O$) as reported by Mortlock and Froelich (1989). Dissolved elements in the supernatant overlying the trap particulate samples were not measured and thus particulate fluxes have not been corrected for total fluxes.

Diatom counting and identification was performed using a full sediment trap sample aliquot (Abrantes et al., 2005). Each sample was first cleaned of organic matter and carbonate by additions of H_2O_2 30% and HCl 10%, respectively. Permanent slides of the entire aliquots (2 fractions <63 μm and >63 μm) were prepared using the evaporation n-tray method (Battarbee, 1973) and the Norland optical adhesive (NOA61) as mounting medium. Diatom counting and species identification was performed at 1000 X (×10 eyepieces and ×100 objectives), using a Nikon Eclipse E100 microscope equipped with Differential Interference Contrast. Exactly 100 randomly-selected fields of view were counted in three replicate slides. For each sample,

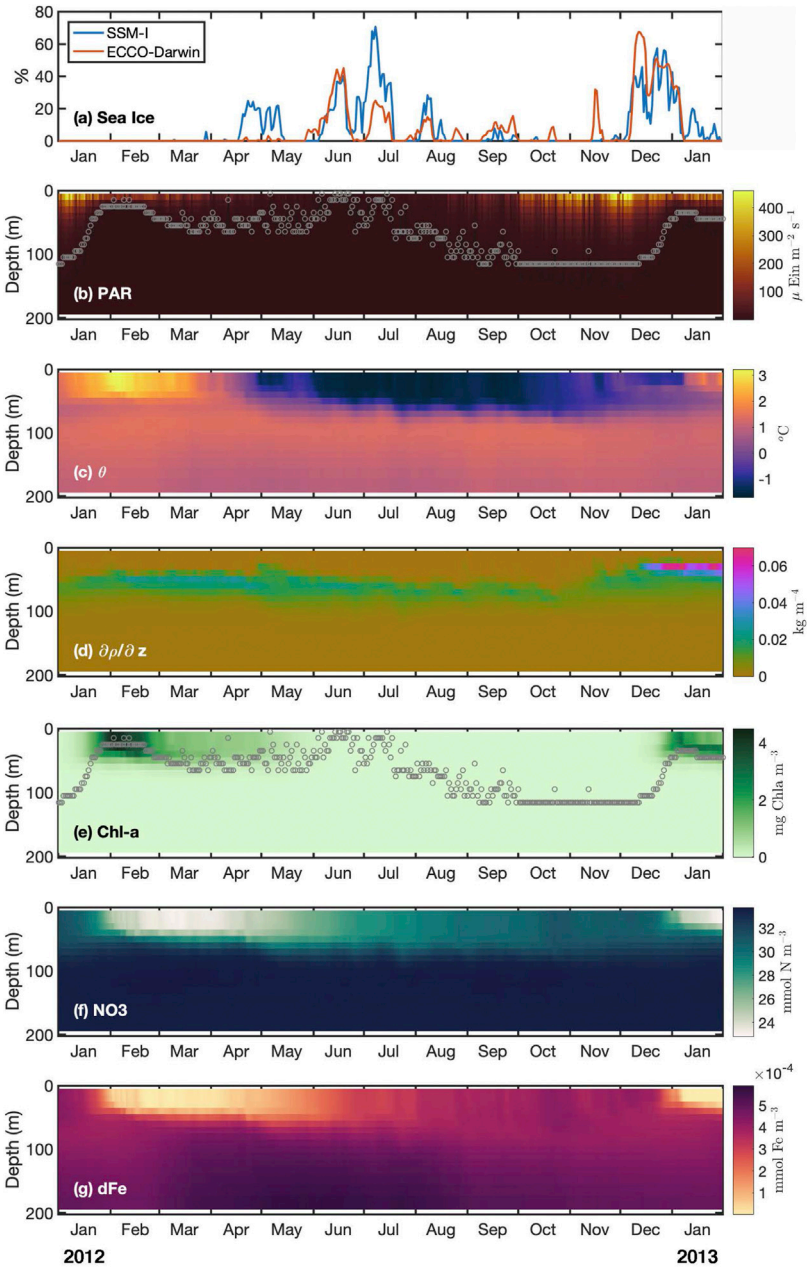

FIGURE 2 | Sea-ice concentration from satellite observations (SSM-I) and environmental variables from ECCO-Darwin at the sediment trap location. **(A)** Sea-ice concentration, **(B)** Photosynthethic Active Radiation (PAR, μ Eins m^{-2} s^{-1}), **(C)** potential temperature, **(D)** stratification (-dρ/dz, kg m^{-4}), **(E)** Chlorophyll *a* (Chl *a*, mg m^{-3}), **(F)** and **(G)** concentration of dissolved nitrate (NO_3, mmol m^{-3}) and dissolved iron (dFe, mmol m^{-3}), respectively. Photic layer depth is shown as gray circles in panels **(B)** and **(E)**.

300 specimens were identified to the species level and raw counts were then converted to percent abundance. Data presented in this work only includes the dominant diatom species, which represent >70% of the total diatom assemblage.

Sea-Ice Concentrations

Sea-ice velocity fields (**Supplementary Figure S1**) were obtained from Tschudi et al. (2016). Sea-ice concentration data for years 2012 and 2013 were obtained from the 89 GHz channels of the AMSR2 satellite microwave radiometer with a grid resolution of 6.25 km (Spreen et al., 2008, data available from www.seaice.uni-bremen.de). Sea-ice concentration anomalies (**Supplementary Figure S2**) were calculated as differences relative to the December 1979–2016 mean sea-ice concentration based on SMMR and SSM/I-SSMIS data at 25 km grid resolution (Cavalieri et al., 2016). The same sea-ice data were also used to calculate sea-ice persistence (**Supplementary Figure S3**) and the sea ice concentration time series in **Figure 2A** for a 75 × 81 km region surrounding the mooring.

ECCO-Darwin

The state-of-the-art ECCO-Darwin ocean biogeochemistry model and its performance has been extensively discussed in the literature (Brix et al., 2015; Manizza et al., 2019; Carroll et al., 2020). ECCO-Darwin is based on a global ocean and sea-ice configuration of the Massachusetts Institute of Technology general circulation model (MITgcm) (Marshall et al., 1997). The physical ocean circulation is from the Estimating the Circulation and Climate of the Ocean (ECCO) consortium (Wunsch et al., 2009), which synthesizes the MITgcm with nearly all available ocean observations since the era of satellite altimetry (~1992), and provides an adjoint-method-based reconstruction of the three-dimensional, time-varying global ocean and sea-ice state. The ECCO circulation estimates are used to drive an online ecosystem model provided by the MIT Darwin Project (Follows et al., 2007; Follows and Dutkiewicz, 2011; Dutkiewicz et al., 2015), which in turn drives and interacts with marine chemistry variables. ECCO-Darwin uses physical fields from the recently released ECCO LLC270 global ocean and sea-ice data synthesis (Zhang et al., 2018); ECCO LLC270 has ~18 km horizontal grid spacing at high latitudes.

The MIT Darwin Project ecosystem model is used to couple the ECCO physical solution with ocean ecology and carbon chemistry (Brix et al., 2015; Manizza et al., 2019; Carroll et al., 2020). Standard ecological equations and parameters (Dutkiewicz et al., 2019) are employed; the Darwin ecology includes five large-to-small phytoplankton function types (diatoms, other large eukaryotes, *Synechococcus*, and low- and high-light adapted *Prochlorococcus*) and two zooplankton types that graze preferentially on either the large eukaryotes or small picoplankton. Biogeochemical tracers (inorganic nutrients, phytoplankton, zooplankton, dissolved organic matter, and detrital particles) are advected and mixed online by the ECCO LLC270 physical fields. The carbon and nitrogen cycle in Darwin is explicitly represented, along with phosphorus, iron, silicon, oxygen, and alkalinity. To provide an estimate of realistic physical and biogeochemical conditions in the water column we use daily model outputs from January 2012 to March 2013, taken at the grid cell closest to the mooring location.

Statistical Analysis

The relationship between the relative abundance of diatom species assemblages and upper-ocean environmental variables obtained from ECCO-Darwin model during the period March 2012 – January 2013 were analyzed using the ordination technique canonical correspondence analysis (CCA) (vegan package, R-project; ter Braak, 1986; Oksanen et al., 2015).

The water-column environmental data used for this exploration is the result of averaging or integrating each value to the photic layer depth after determining the depth where photosynthetic available radiation (PAR) is 1% of its surface value and above a minimum threshold of 1 μ Ein m^{-2} s^{-1} (**Table 1**).

Preliminary variable reduction was carried out through hierarchical cluster analysis using euclidean distance, principal component analysis, and correlation matrix plots, which were used to determine the main groups of variables (not shown for brevity). Within each main group, a representative variable was selected, based on the relationship with other variables and on previous scientific knowledge, to avoid issues with collinearity and for variable reduction. Thus, for the final analysis, sampling time (month), temperature (temp), sea-ice concentration (seaice), dissolved iron (dFe), stratification (strat), particulate organic carbon (POC), Photosynthethic Active Radiation (PAR) and chlorophyll *a* (chl) were considered. The effect of multicollinearity of environmental variables was checked after modeling using variance inflation factors (VIFs) applied to the CCA. For the species matrix, Hellinger distance was used, as recommended for community compositional data (Legendre and Gallagher, 2001). Significant environmental variables were identified *via* a stepwise procedure, using permutation tests (999 permutations). After the selection of the significant variables, the model was tested a second time through a Monte Carlo global permutation test (999 permutations) to assess the significance of ordination axes, partial terms and global model.

The results of the CCA are presented as an ordination triplot diagram containing the explanatory variables plotted as arrows along with numbers for samples (dates) and diatom species (main groups of diatoms). All statistical analysis was carried out using r-project (ter Braak, 1986; Oksanen et al., 2015).

RESULTS

Environmental Data and Water-Column Characteristics From ECCO-Darwin

We first use ECCO-Darwin, which provides a best-possible estimate of the global-ocean state by assimilating both physical and biogeochemical observation to infer the environmental conditions and the associated seasonal variability at the mooring location during 2012–2013. Larger concentrations of sea ice were observed in June–July 2012 and in December 2012 (**Figure 2A**), when sea ice was advected into the study region from the Weddell Sea (**Supplementary Figure S1**). Sea ice is typically present in the area during austral winter but not in summer. In December 2012 the sea-ice edge was located 200–300 km northward from its typical location, causing the study area to be anomalously covered by 30% sea-ice concentration (**Supplementary Figure S2**). The sea-ice anomaly was such that in over 38 years of satellite data, sea ice was never observed in the area during December (**Supplementary Figure S3**).

Sea-ice concentration from ECCO-Darwin showed general agreement with satellite observations (**Figure 2A**). Upper-ocean properties (surface to 150-m depth) extracted from ECCO-Darwin at the mooring location are shown in **Figure 2** and **Table 1**. Relatively high PAR was observed in austral spring and summer months (January – March 2012, and from October 2012 to January 2013; **Figure 2B**) due to net heat gain from the atmosphere into the ocean. Mean ocean temperatures within the photic layer ranged between −0.1 and 1.8°C and presented maximum values in concordance with high PAR and absence of sea ice (**Figures 2A–C** and **Table 1**). The relatively low stratification increased three-fold in January 2013, due to sea-

TABLE 1 | Water-column environmental variables obtained from ECCO-Darwin at the mooring location. Daily data were averaged (indicated with *) or integrated within the photic layer depth after determining the depth at which photosynthetic available radiation (PAR) equals 1% of its surface value, and above a minimum threshold of 1 μ Ein m^{-2} s^{-1}. Data was subsequently averaged over the time interval corresponding to each trap sample (code E1 to E11). PAR: Photosynthethic Active Radiation; MLD, mixed layer depth; Temp, potential temperature; Sal, salinity; Strat, stratification; NO3, nitrate concentration; PO4, phosphate concentration; SiO_2, silicate concentration; dFe, total dissolved iron concentration; bioSi/OC, biogenic silicon/organic carbon molar ratio; Chl *a*, chlorophyll *a* concentration.

	Date	PAR	MLD	Temp*	Sal*	Strat*	NO3	PO4	SiO4	dFe	bioSi/OC*	Chla
		(μ Ein m-2 s-1)	(m)	(°C)		(kg m-4)	(mmol m-3)	(mmol m-3)	(mmol m-3)	(mmol m–3)	(mol:mol)	(mg Chla m–3)
E1	March 16, 2012	159.1	30	1.81	33.71	-0.0085	150.2	10.8	393.2	0.70	0.450	6.35
E2	April 16, 2012	71.5	28	0.59	33.60	-0.0074	143.7	10.3	364.4	0.74	0.450	4.18
E3	May 16, 2012	33.4	23	–0.61	33.41	–0.0063	140.3	10.0	349.5	0.93	0.449	1.61
E4	June 16, 2012	7.4	33	–1.50	33.42	–0.0009	81.3	5.8	207.9	0.75	0.449	0.12
E5	July 16, 2012	21.9	38	–1.41	33.62	–0.0021	138.2	9.7	314.1	1.53	0.451	0.01
E6	August 16, 2012	76.8	39	–0.88	33.86	–0.0041	250.4	17.5	567.8	3.08	0.452	0.00
E7	September 16, 2012	186.9	36	–0.37	34.00	–0.0043	327.5	22.8	729.0	4.11	0.452	0.00
E8	October 16, 2012	601.0	44	–0.06	34.10	–0.0035	380.3	26.5	857.1	4.95	0.451	0.00
E9	November 16, 2012	801.4	26	0.15	34.05	–0.0048	383.1	26.7	842.8	4.86	0.450	0.01
E10	December 16, 2012	705.5	12	0.20	33.81	–0.0111	325.7	22.7	715.6	3.95	0.448	1.85
E11	January 12, 2013	290.5	13	0.45	33.17	–0.0234	121.3	8.6	289.7	0.70	0.448	8.52

ice melt (**Figure 2D**). Spring-summer peaks of Chl *a* between second half of January–March 2012 and January 2013 were associated with dissolved iron and nitrate consumption by model phytoplankton (**Figures 2E–G**).

Sinking Particulate Material Time Series

Biosiliceous organism fluxes at 1000-m depth ranged between a maximum of 5.6 10^6 valves $m^{-2}d^{-1}$ in June 2012 to a minimum of 2.5 10^6 valves $m^{-2}d^{-1}$ in September 2012 (**Figure 3A**). Diatoms dominated the total siliceous microorganisms during all months, whilst silicoflagellates constitute less than 1% (**Figure 3A**). Diatom fluxes averaged 3.5 10^6 valves $m^{-2}d^{-1}$ and showed marked inter-month variability in terms of assemblage. The large-sized diatom *Corethron pennatum* (Grunow) Ostenfeld (diameter ~47 μm; pervalvar axis ~149 μm) (Annett et al., 2010) and *Chaetoceros* sp. resting spores were dominant during summer (March 2012 and December 2012–January 2013), reaching up to 67% (January 2013) and 25% (March 2012) of the total flux, respectively (**Figures 3B**, **4A,D**). Thalassiosira gracilis (Karsten) Hustedt became more abundant during winter, representing up to 43% of the total diatom flux in June 2012 (**Figures 3B**, **4C**). The diatom assemblage in sinking particles was also explained by the highly silicified *Fragilariopsis kerguelensis* (O'Meara) Hustedt (whose relative contribution remained relatively constant throughout the year, ~26%), the sea-ice related species Fragilariopsis curta (Van Heurck) Hustedt and Fragilariopsis cylindrus (Grunow ex Cleve) Helmcke and Krieger (<7% on average), and the large O*odontellaceae* diatom *Odontella weissflogii* (Grunow) Grunow (reached up to 7%) (**Figures 3B**, **4B,E,F**).

OC and bioSi fluxes varied around averages of 1.53 mmol OC $m^{-2}d^{-1}$ and 2.86 mmol bioSi $m^{-2}d^{-1}$, respectively, and showed clear differences between months (**Figure 3C** and **Table 2**). OC represented 1–2.3% of the total mass flux, and varied from minimum OC values of 0.76 mmol OC $m^{-2}d^{-1}$ in August 2012 to maximum values of 2.38 mmol OC $m^{-2}d^{-1}$ in March 2012. bioSi fluxes were also higher in summer months, especially in December 2012, when bioSi fluxes achieved a maximum of 6.82 bioSi $m^{-2}d^{-1}$ (**Figure 3C** and **Table 2**). Furthermore, the bioSi/OC ratio that varied around a mean of 1.8 showed marked differences during the year, with a maximum of 2.95 in December 2012 (**Figure 3D** and **Table 2**). The carbon ($\delta^{13}C$) and nitrogen ($\delta^{15}N$) isotopic signal of sinking particles varied around mean values of −27.52 and 2.24, respectively; these also showed significant differences over the study period, with summer samples characterized by lower values compared to winter samples (**Figure 3E** and **Table 2**).

Relationships Between Sediment Trap Data and Modeled Environmental Variables

canonical correspondence analysis (CCA; **Figure 5**) evidenced the importance of both 1) upper-ocean hydrographic conditions and 2) sea-ice concentration, in determining diatom species assemblages collected by the sediment trap. The initial model CCA included: Photosynthethic Active Radiation (PAR), sea-ice concentration (sea ice), temperature, dissolved iron (dFe), stratification, chlorophyll a (chl), and particulate organic carbon (POC). POC was excluded due to VIF results, whereas PAR and Chl *a* were excluded on the stepwise procedure from the CCA analysis, due to non significance and low contribution to the model. The CCA final model with only four variables (stratification, temperature, sea ice, and dissolved iron content) explained 89% of the total variance in the species assemblage (adjusted R^2) (**Figure 5**). The model was significant (F = 21.064 m

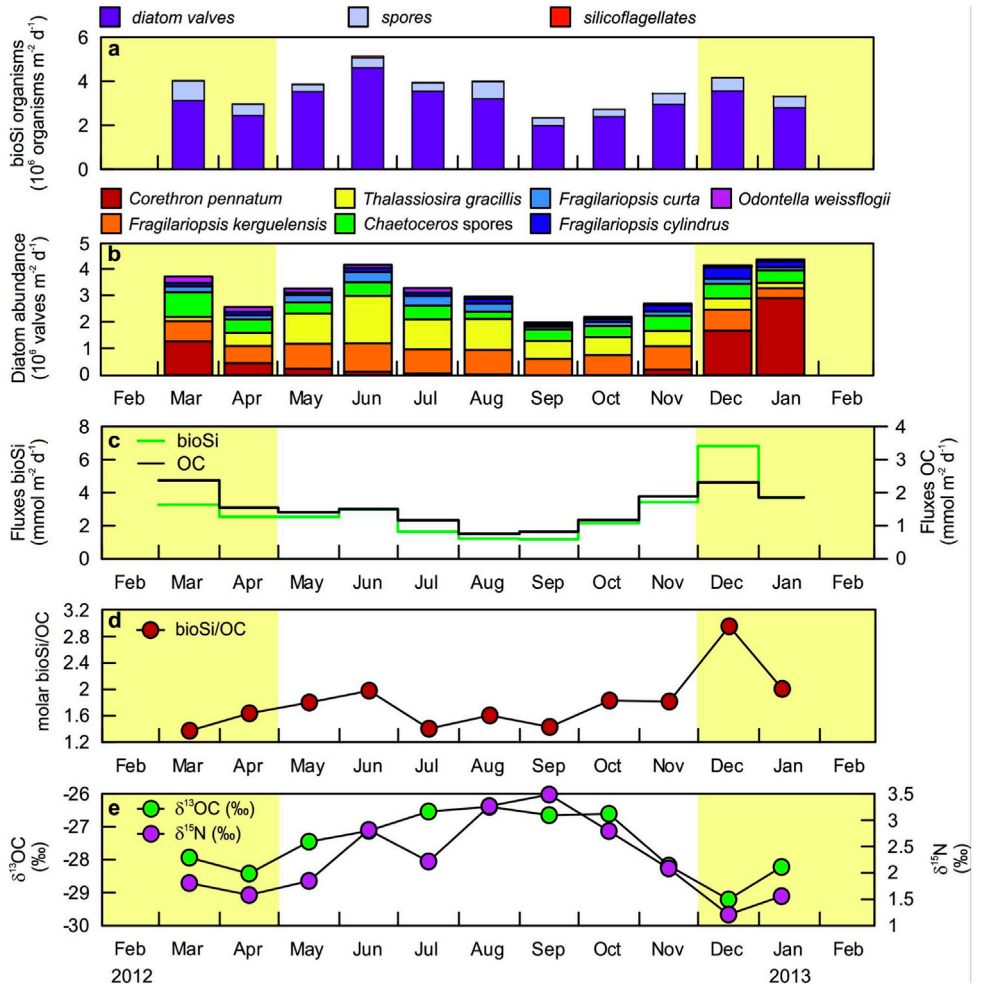

FIGURE 3 | Time series for biosiliceous organisms, diatom assemblage and biogeochemical signals of the settling material recovered by a sediment trap at 1,000 m depth in 2012/13. **(A)** Total biosiliceous (bioSi) organisms. **(B)** main diatom species abundance. **(C)** Fluxes of biogenic silicon (bioSi) and organic carbon (OC). **(D)** OC normalized bioSi molar ratio. **(E)** Stable isotope ratios of C (δ^{13}OC) and N (δ^{15}N). Shaded areas correspond to periods with relatively high Chl *a* concentration in the upper photic layer according to ECCO-Darwin model data (see **Figure 2E**).

p = 0.001), as well as the four environmental terms, with iron being marginally significant (F = 4.38, p = 0.06). The first two axes explained 85 and 5% respectively. Variance inflation factors (VIF) of the four terms were all below two.

The first canonical axis is primarily associated with temperature and stratification. The analysis discriminates between high/low productivity conditions, along with the species associated with each season. Month 1 (January 2013) is representative of a highly-productive period associated with *Corethron pennatum*. Months 6 (June 2012), 8 (August 2012), 9 (September 2012), and 10 (October 2012) correspond to periods of low productivity, associated with *T. gracillis, F. cylindrus,* and *F. curta*. The second canonical axis reflects sea-ice concentration and shows a separation of species associated with sea-ice in summer (*C. pennatum*) and winter (*T. gracillis*, *F. cylindrus,* and *F. curta*) from species less impacted by sea ice (*Chaetoceros* spores and *Odontella weissflogii*). Note also that the oceanographic variables were associated with the first canonical axis, explaining 85% of the variability in species assemblages, whereas sea ice, associated with the second axis, represents only 5% of the species assemblage variability.

DISCUSSION

Biosiliceous organisms sinking at 1,000 m depth in the South Scotia Ridge -a naturally Fe-enriched region (Fugre 1)-, were primarily represented by diatom valves (**Figure 3A**). Silicoflagellates contributed only a small fraction (mean of 0.6%), and based on previous studies, radiolarians, another key contributor to biogenic silicon fluxes, appear in minor proportions in our study site (less than 1%) (Gersonde and Wefer, 1987; Abelmann and Gersonde, 1991). Our data thus corroborates that diatoms are the largest contributors of bioSi fluxes in the study area.

The fact that diatom assemblages observed at depth were primarily composed of heavily silicified species

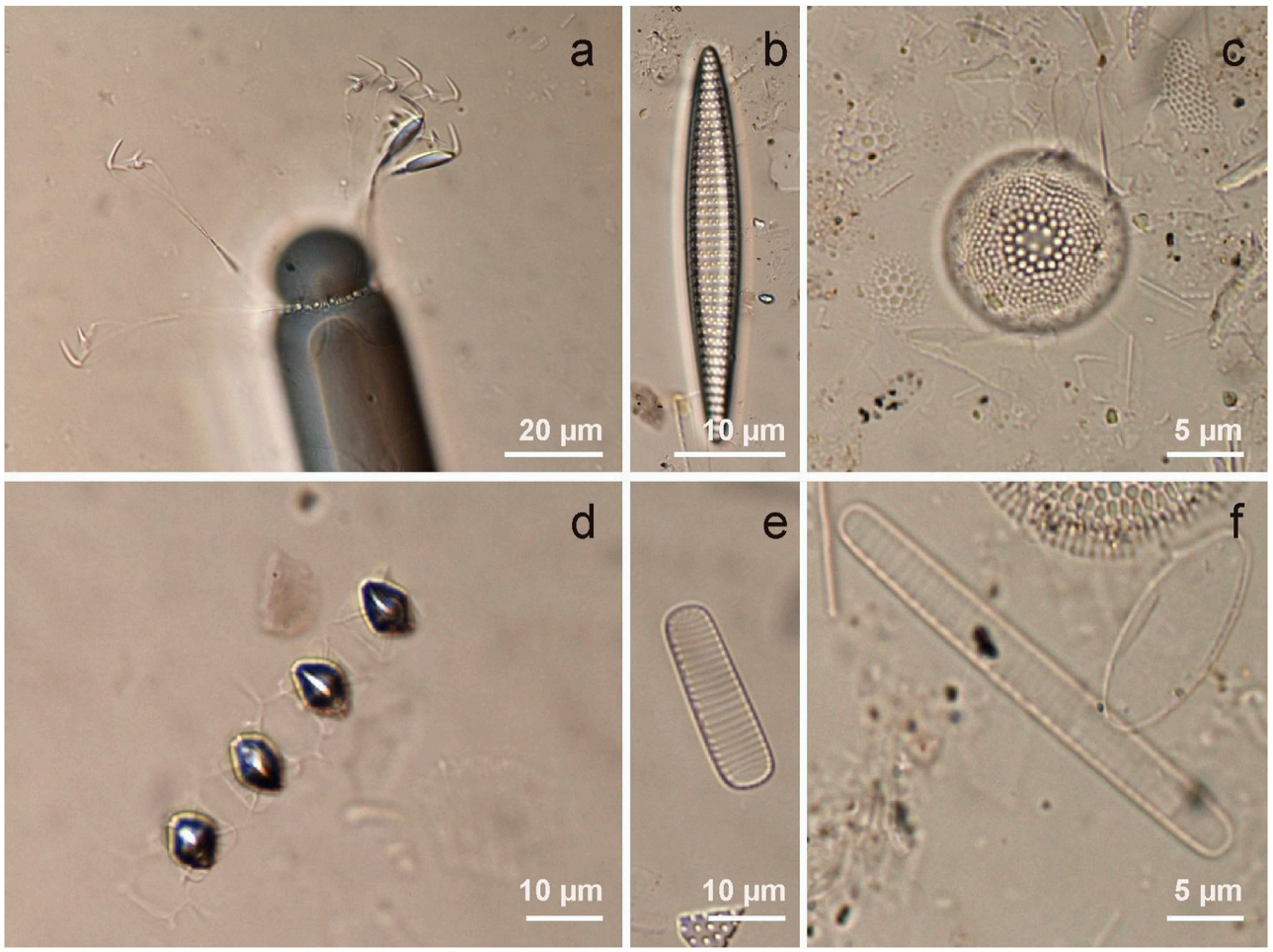

FIGURE 4 | Main diatom species found by microscope examination of the sediment trap samples (<63 µm and >63 µm fractions). **(A)** *Corethron pennatum*. **(B)** *Fragilariopsis kerguelensis.* **(C)** *Thalassiosira gracilis*. **(D)** *Chaetoceros* sp. resting spores. **(E)** *Fragilariopsis curta*. **(F)** *Fragilariopsis cylindrus*).

TABLE 2 | Total mass fluxes (TMF), fluxes and concentrations of main components (OC, organic carbon; IC, inorganic carbon; bioSi, biogenic silicon) and lithogenics (litho). The C and N isotope ratios ($\delta^{13}C$ and $\delta^{15}N$), and molar bioSi/OC ratio are also presented.

	Date	TMF	OC	OC	IC	IC	bioSi	bioSi	Litho	Litho flux	$\delta^{13}C$	$\delta^{15}N$	bioSi/OC
		(mg $m^{-2}d^{-1}$)	%	(mmol $m^{-2}d^{-1}$)	%	(mmol $m^{-2}d^{-1}$)	%	(mmol $m^{-2}d^{-1}$)	%	(mg $m^{-2}d^{-1}$)	(‰)	(‰)	molar
E1	March 16, 2012	1230.45	2.32%	2.38	0.21%	0.21	7.43%	3.26	75.79%	932.54	–27.94	1.81	1.37
E2	April 16, 2012	826.60	2.25%	1.55	0.58%	0.40	8.61%	2.53	69.98%	578.45	–28.42	1.58	1.63
E3	May 16, 2012	1028.76	1.64%	1.41	0.14%	0.12	6.90%	2.53	78.97%	812.40	–27.45	1.85	1.80
E4	June 16, 2012	1560.22	1.16%	1.51	0.14%	0.18	5.35%	2.97	83.65%	1305.14	–27.12	2.82	1.98
E5	July 16, 2012	1097.53	1.28%	1.17	0.18%	0.17	4.19%	1.64	85.87%	942.41	–26.54	2.22	1.40
E6	August 16, 2012	886.28	1.03%	0.76	0.21%	0.16	3.86%	1.22	86.90%	770.18	–26.39	3.27	1.60
E7	September 16, 2012	741.11	1.34%	0.82	0.21%	0.13	4.46%	1.18	84.87%	628.99	–26.65	3.48	1.43
E8	October 16, 2012	892.53	1.58%	1.18	0.19%	0.14	6.76%	2.15	79.01%	705.17	–26.61	2.79	1.83
E9	November 16, 2012	1041.74	2.18%	1.89	0.15%	0.13	9.23%	3.42	72.22%	752.38	–28.18	2.08	1.81
E10	December 16, 2012	1410.86	1.97%	2.31	0.25%	0.30	13.57%	6.82	61.38%	865.94	–29.21	1.21	2.95
E11	January 12, 2013	1227.85	1.81%	1.86	0.44%	0.45	8.50%	3.72	72.34%	888.21	–28.22	1.56	2.00

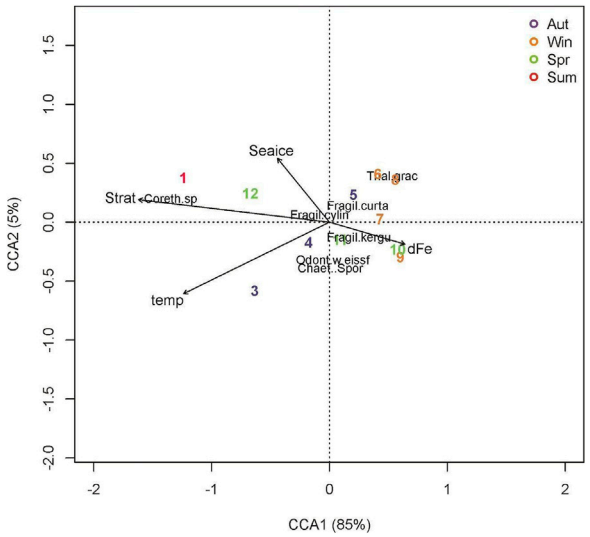

FIGURE 5 | RDA triplot results of the final canonical correspondence analysis (CCA) for the most relevant fossil diatom species registered in our sediment trap during the period March 2012-January 2013 (*Corethron pennatum*: Coreth. sp; *Chaetoceros* spores: Chaet. Spor.; *Fragilariopsis kerguelensis*: Fragil. kergu.; *Thalassiosira gracilis*: Tha. grac; *Fragilariopsis curta*: Fragil. curta; *Fragilariopsis cylindrus*: Fragil. cylin; *Odontella weisflogii:* Odont. weissf), and environmental variables (Seaice: sea ice; Strat: stratification; temp; temperature; dFe: dissolved iron). Numbers from 1 to 12 represent months from January–December. Aut: autumn (purple); Win: winter (orange); Spr: spring (green); Sum: summer (red).

with well-preserved valves (**Figure 4**) highlights the role of silicification in export production, as less-silicified species may be more prone to dissolution in the upper-water column (Annett et al., 2010). We note that other diatom survival strategies such as their huge size (e.g., *C. pennatum*; **Figure 4A**) or the formation of chains (e.g., *F. kerguelensis;* **Figure 4B**) may also protect diatoms against grazing pressure (Hamm et al., 2003; Smetacek et al., 2004), and thus aiding in their ability to reach deep waters. However, the observation of small fragments during microscopic analysis also suggests the presence of less-silicified species, likely affected by dissolution during vertical export (Abelmann and Gersonde, 1991). In this regard, Nelson and Gordon (1982) estimated that, in the SO, up to 18–58% of biogenic opal might be dissolved in the upper 100 m. This implies that our bioSi content, which does not exceed 14% of the total flux (**Table 2**), could represent a relatively small fraction of the bioSi in the productive upper water column.

Diatom assemblage in sinking particles appear to have a major role in setting OC and bioSi export rates during our experiment year, with mean fluxes of 1.53 mmol OC $m^{-2}d^{-1}$ and 2.86 mmol bioSi m^{-2} d^{-1} (**Figure 3C** and **Table 2**)—these are in the higher range of those reported for the SO at 1000-m depth (Honjo, 2004). Strong evidence that enhanced settling of biogenic compounds occurred in close correlation with primary production in the upper water column is provided by the fact that lithogenic fluxes, as a tracer of the input of continental particles, even representing a significant fraction of the sinking material (**Table 2**), were not correlated with either OC nor bioSi fluxes (r^2 = 0.07 and r^2 = 0.05, respectively; **Supplementary Figure S4**). Instead, sinking OC was closely related to bioSi downward flux (r^2 = 0.7; **Supplementary Figure S4**), suggesting that both biogenic compounds are closely linked to diatom's production. This finding and the high proportion of well-preserved valves in the samples also suggests that the majority of diatoms recorded at depth sank from the surface, either as solitary cells or as part of fast-sinking fecal pellets and aggregates (i.e., Smetacek, 1985; Manno et al., 2015). In spite of that, OC and bioSi behave differently during their way down to the bottom. The higher bioSi/OC molar ratios in settling material (mean value of 1.8) when compared with those from ECCO-Darwin in the photic layer (average of ~0.4) (**Table 1** and **Table 2**), point to a preferential export of bioSi relative to OC (DeMaster, 2002; Rembauville et al., 2016). Against this background, Pilskaln et al. (2004) show that the OC exported to 1000-m depth in the SO may represent only 1% of the annual OC production in surface waters, while the preservation efficiency for bioSi is 19%. This means that deep particle fluxes obtained with sediment traps need to be carefully interpreted when attributing OC and bioSi export rates directly to exported particles and diatoms sinking.

Seasonal Succession of Diatoms Assemblage Determining bioSi/OC Variations

OC sinking fluxes down to 1000-m depth were significantly higher during austral summer periods, reflecting the end of the 2012 bloom and the early summer 2012–2013 in agreement with ECCO-Darwin Chl a concentrations (**Figures 2E**, **3C**). The diatom assemblages during these productive periods were principally explained by two bloom-forming diatoms: *Chaetoceros* spp. (represented by their resting spores) and the giant *C. pennatum* (**Figure 3B**). The chain-forming, highly-silicified *Fragilariopsis kerguelensis* also achieved significant proportions (maximum of 25%) during those intervals. This structure of the diatom's community corroborates that OC sequestration was characterized by species that build up high biomass under favorable growth conditions (e.g., *Chaetoceros* and *C. pennatum*) rather than species whose survival strategy is based on the maintenance of relatively constant stocks throughout the year (*F. kerguelensis*) (Smetacek et al., 2002; Timmermans et al., 2004; Peloquin and Smith, 2006).

Corethron pennatum fluxes seems to reflect both the end of the 2012 and the early summer 2012–13 blooms (**Figures 2E**, **3B**). Indeed, the high correlation of *C. pennatum* abundances and δ^{13}OC and δ^{15}N isotopic signals (r^2 = 0.76 and r^2 = 0.77, respectively; **Supplementary Figure S4**) points to this species exert an important role in determining biogeochemical signature of the sinking organic matter (**Figures 3B,E**). This is consistent with previous findings that show a lowering δ^{13}C (−30–−32) of settling OC when *C. pennatum* dominates (Bathmann et al., 1991). Moreover, our data agrees with *in-situ* observations at Marguerite Bay (West Antarctic Peninsula) that attribute the shift in δ^{13}OC isotopic signals of sinking material to contrasting

carbon utilization mechanisms by different diatom species (Henley et al., 2012; Shen et al., 2017).

However, we found some differences in how diatoms community structure regulate bioSi/OC molar ratio during these highly productive periods. In March 2012, despite *Corethron pennatum* is a relevant species, the comparatively high contribution of dense *Chaetoceros* spp. resting spores during this month may explain the relatively low bioSi/OC molar ratio (~1.4) (**Figures 3B,D**). The reduction in this ratio due to enhanced carbon export by diatom resting spores has been observed in other Fe-rich regions of the SO (Salter et al., 2012; Rembauville et al., 2016). In contrast, during early summer 2012–2013, we found a relatively higher export of bioSi relative to OC (**Figure 3D**). The relatively low Chl a during December 2012, coinciding with the arrival of sea ice to our study site, suggests that in addition to the onset of the *Corethron pennatum* bloom (**Figures 2A**,E, **3B**), the high bioSi export occurring during this month might be also explained by advective processes (Abelmann and Gersonde, 1991). The particular increase of the diatom species *F. cylindrus*, which is associated with coastal regions of Antarctica and consolidated sea ice, would also support this hypothesis (Armand et al., 2005; Lundholm and Hasle, 2008). However, the January 2013 maximum in Chl a in the photic layer, which coincide with the massive bloom of *C. pennatum* (**Figures 2E**, **3B**,D) indicates that this large diatom has a significant role in favoring the export of bioSi relatively to OC to the deep ocean (bioSi/OC ratio close to two).

Environmental Factors in the Upper Photic Layer Triggering Seasonal Diatom Assemblage

Environmental conditions from ECCO-Darwin show a seasonal productivity pattern in the photic layer with a maximum of Chl a occurring during summer, in agreement with low macronutrients levels reflecting phytoplankton consumption (**Figures 2E,F**). Modeled Chl *a* and nutrient concentrations generally agree with field data previously obtained near our study site (Korb et al., 2005; Ardelan et al., 2010). The model also reproduces the consumption of dissolved Fe associated with increased summer productivity in the upper layer (**Figure 2G**), although the dFe background levels of ~0.4 nM are typical of non Fe-limited regions (Dulaiova et al., 2009; DeJong et al., 2012; Measures et al., 2013). The Fe-enrichment in this study area is primarily attributed to the arrival of shelf waters from the Antarctic Peninsula (Hatta et al., 2013; Klunder et al., 2014). Additionally, local sea-ice melt -as occurred in January 2013-, is another known source of dissolved Fe in this region (Wang et al., 2014; Lannuzel and Chever, 2016; Monien et al., 2017).

Sinking diatom assemblages, which follow the seasonal trend of environmental variables in the upper photic layer was reflected in the ordination technique canonical correspondence analysis, where we assume that sinking rates are high enough for the particles to sink to 1,000 m depth in less than 30 days (**Figure 5**). This assumption has been considered in previous SO studies (e.g., Pilskaln et al., 2004; Fisher and Karakaç, 2009; Rigual-Hernandez et al., 2019). Considering this, our analysis shows that, apart from irradiance and dFe, other environmental factors such as water column stratification of the water column need to be considered as triggers of phytoplankton blooms. This means that increased stratification, whether it occurs at the end of summer due to heating of the surface layer (March-April 2012), or it is associated with sea ice melt, as occurred in early summer 2012–2013, plays a key role in promoting *C. pennatum* blooms (**Figures 2D**, **3B**, **5**). Such massive blooms have been previously observed close to our study site (Gersonde and (Wefer, 1987; Fryxell, 1989) as well as in the vicinity of South Georgia Island (Froneman et al., 1995, 1997), and at frontal zones in the Atlantic sector of the SO (Laubscher et al., 1993; Bathmann et al., 1997). Our data suggests that sea ice may trigger an early summer bloom, as recently observed in the Arctic Ocean (Boetius et al., 2013; Clement-Kinney et al., 2020). This may occur *via* two main processes. First, local melting of sea ice can result in an additional flux of dissolved nutrients (such as Fe) to near-surface waters (Lannuzel and Chever, 2016). This might provide the extra nutrient supply needed to promote blooms and the high ambient Fe concentrations required by the large, slow growing *C. pennatum* to reach optimal growth rates (Timmermans et al., 2004; Smetacek et al., 2004; Hoffmann et al., 2006). Second, the capacity of *C. pennatum* to adjust its buoyancy would provide an advantage for exploiting nutrients in stratified waters, allowing for blooms under low-light conditions (as reproduced by ECCO-Darwin; **Figure 2B**). Though *C. pennatum* buoyancy adjustment has only been reported by Crawford (1995), this mechanism was observed for other large diatoms (e.g. *Rhizosolenia* and *Proboscia*) (Villareal et al., 1993, 1999a, 1999b; Moore and Villareal, 1996; Singler and Villareal, 2005; Kemp et al., 2006). This supports the idea that *Corethron* might also be adapted to exploit a stratified water column (via sea ice melt) and deep nutrient sources. In this context, Chl *a* maxima associated with sea-ice melt was attributed to *C. pennatum* in the Atlantic sector of the SO (Fryxell, 1989), and in the South Georgia region (Whitehouse et al., 2008; Nunes et al., 2019). The blooming of this large diatom, combined with its morphological characteristics (such as the presence of a set of shorted barbed spines that favor entanglement and aggregation, or its large size that allow scape grazing, probably favor larger export into the deep ocean (Smetacek, 1985; Alldredge and Gotschalk, 1989; Smetacek et al., 2004). Increased sinking of *C. pennatum* half-cell walls may occur due to the fall-down of a sexual reproductive phase event (Crawford, 1995), but the absence of half-cells in the samples prevent us from confirming this hypothesis. Accordingly, this data supports the assumption used by paleoceanographers where *C. pennatum* creates and rapidly exports substantial biomass under stratified conditions during times of enhanced sea-ice melt (Jordan et al., 1991; Leventer et al., 1993; Sedwick et al., 2001; Leventer et al., 2002; Taylor and Sjunneskog, 2002; Maddison et al., 2012; Alley et al., 2018).

The role of stratification in promoting *C. pennatum* blooms is also supported by the observed changes in the sinking organic matter total nitrogen (TN) and OC isotopic composition, which are well-established proxies for assimilation of surface-ocean nitrate and dissolved inorganic carbon (DIC) by phytoplankton (Sigman et al., 1999). Exported organic matter shows relatively low $\delta^{15}N$ values (1.2–1.6‰) in periods when *C. pennatum* dominates the diatoms assemblage (**Figures 3B,E**). These values are significantly lower than the typical summer $\delta^{15}N$ values of surface-ocean nitrate (>5‰) (Sigman et al., 2000), suggesting a shift from high $\delta^{15}N$ -NO3 to low $\delta^{15}N$ -NH_4^+ as the primary nitrogen source exploitable by these large

blooming diatoms. However, this does not agree with the assumption that NH_4^+-assimilating phytoplankton are typically smaller in size (Berg et al., 2011). Another possibility is that phytoplankton utilize under-ice NH_4^+ and DIC with low $\delta^{13}C$ (because of low ventilation). However, low $\delta^{15}N$ and $\delta^{13}OC$ were also recorded during sea-ice free conditions in February 2012. Yet, the robust positive correlation of $\delta^{13}OC$ and $\delta^{15}N$ (r^2 = 0.74; **Supplementary Figure S4**) suggests that the mechanism responsible for low $\delta^{15}N$ is also decreasing the $\delta^{13}OC$ of sinking particles. If assimilation of low ^{13}OC DIC relatively to ambient DIC occurs deeper in the water column, then vertical migration due to buoyancy regulation of *C. pennatum* would also explain the use of lighter ^{14}N from the nutricline and near-surface waters, triggering lower $\delta^{15}N$ in settling particles.

CONCLUSION

Settling material collected by a sediment trap at 1000 m depth in the South Scotia Ridge provides, for the first time, an almost complete annual cycle of diatom abundance and composition in the southern sector of the Scotia Sea. A statistical analysis of in-situ data and realistic ocean biogeochemistry simulation shows that the material collected by the sediment trap reflects changes in upper-ocean environmental conditions. Additionally, sediment trap data provide geochemical evidence that massive *C. pennatum* blooms occuring in highly-stratified waters thrive during early summer sea-ice melt conditions. Consequently, the sedimentation of these large diatoms enhance silicon removal from SO waters. Our results, together with similar studies that report high bioSi/OC ratios in other Fe-rich SO regions, challenge the conventional view of diatoms growing under Fe-replete conditions as drivers of sinking high OC to bioSi fluxes. We conclude that, along with irradiance and dFe, sea ice concentration (which modulates changes in upper-ocean stratification), needs to be considered when determining which environmental factors trigger specific diatoms blooms, that, in turn, determine carbon sequestration. To our knowledge, this is a novel aspect of diatoms ecology in setting bioSi vs. OC sequestration efficiency—a key controlling factor that regulates the stoichiometric relationship of limiting nutrients for primary production. Ultimately, additional studies that combine water column environmental conditions and surface-to-bottom sediment trap data are required to improve our understanding of diatom dynamics and the coupled physical-biogeochemical processes that regulate export in the Southern Ocean.

DATA AVAILABILITY STATEMENT

The datasets presented in this study can be found in online repositories. The names of the repository/repositories and accession number(s) can be found below: The datasets analyzed for this study have been deposited at the Spanish National Polar Data Center (CNDP), http://hielo.igme.es/index.php/en/. ECCO-Darwin model fields are available at: https://data.nas.nasa.gov/ecco.

AUTHOR CONTRIBUTIONS

DZ, AS-V and MMF contributed equally to the writing of the manuscript. MMF conceived, designed the monitoring experiment and acquired the data. AS-V. performed biogeochemical analyses and acquired the data. DZ counted and identified diatom assemblage. DC provided ECCO-Darwin time series and helped with manuscript editing and figure creation. MR performed the statistical analysis. FA provided relevant information for diatoms identification and contributed to the writing of the manuscript. GS contributed with sea-ice analysis and prepared **Supplementary Figures S1–S3**. TC contributed to the writting of the manuscript and provide valuable support during the whole process. All authors read, edited, and approved the final version of the manuscript.

FUNDING

This work was funded by the Spanish Polar Program through the Spanish Research and Innovation (I+D+i) National Plan (grant numbers CTM2009-08287-E/ANT and CTM2011-14056-E/ANT), and supported by the Catalan Government Grups de Recerca Consolidats Grant (2017 SGR 315) and the Internal Research and Technology Development program of the Jet Propulsion Laboratory, California Institute of Technology. DZ was funded by a postdoctoral fellowship (Plan I2C) from Xunta de Galicia (Spain) and performed diatom analysis during her stay at Instituto Português do Mar e da Atmosfera (IPMA), Lisbon, Portugal. Diatom analysis was sponsored by Portuguese national funding through FCT-Fundação para a Ciência e a Tecnologia (UIDB/04326/2020 and DiatBIo PTDC/AAG-GLO/3737/2012 projects). GS was supported by the Deutsche Forschungsgemeinschaft (DFG) in the framework of the priority programme "Antarctic Research with comparative investigations in Arctic ice areas" SPP 1158 by Grant SITAnt (365778379).

ACKNOWLEDGMENTS

The authors are deeply grateful to Joan Puigdefàbregas and Jordi Cateura for their technical assistance in mooring deployment and recovery; Rut Pedrosa-Pàmies and Montse Guart for their help with analytical tasks; the Captain and crew of the R/V Hespérides for their support during the 2012 and 2013 Antarctic cruises.

SUPPLEMENTARY MATERIAL

The Supplementary Material for this article can be found online at: https://www.frontiersin.org/articles/10.3389/feart.2021.579198/full#supplementary-material

Supplementary Figure 1 | Sea ice velocity fields for the months of November 2012, December 2012 and January 2013 obtained from the NASA National Snow and Ice Data Center Distributed Active Archive Center (Tschudi et al.,

2016). Sea ice was strongly advected into the study area during November and December, and the advection stopped in January.

Supplementary Figure 2 | December 2012 sea ice concentration anomaly relative to the reference period 1979–2016. Antarctic Circumpolar Current fronts, after Orsi et al. (1995), are indicated as dashed contours (names labeled). The sediment trap location (60° 24'S; 52° 58'W) is marked by a black star. Gray lines mark parallels and meridians.

Supplementary Figure 3 | Sea ice persistence for the month of December during the 1979–2016 period. Sea-ice persistence gives the frequency of sea ice occurrence (how often sea ice is present) at a given location. Sea ice persistence of 100% means that the area was always covered by sea ice throughout December within the 38-year period 1979–2016; 0% means the opposite: no sea ice was ever present. The mooring location is marked with a star. Sea ice persistence at the mooring location is 2% or 24 days, i.e., 2012 was the only year in which sea ice was observed at that location during the month of December.

Supplementary Figure 4 | Pearson correlation matrix for the sediment trap data. Lithog flux: lithogenic flux (mmol m^{-2} d^{-1}), OC: organic carbon flux (mmol m^{-2} d^{-1}) and relative contribution (%), bioSi: biogenic silicon flux (mmol m^{-2} d^{-1}) and relative contribution (%), biogeochemical variables (d13C= organic carbon isotope ratio; d15N= total nitrogen isotope ratio; bioSi/OC: biogenic silicon/organic carbon molar ratio), and most representative fossil diatoms species (*Corethron pennatum*: Coreth. sp; *Chaetoceros spores*: Chaet.Spor.; *Fragilariopsis kerguelensis*: Fragil.kergu.; *Thalassiosira gracilis*: Thal.grac; *Fragilariopsis curta*: Fragil. curta; *Fragilariopsis cylindrus*: Fragil. cylin; *Odontella weisflogii*: Odont.weissf) abundances expressed in valves m^{-2} d^{-1}).

REFERENCES

Abelmann, A., and Gersonde, R. (1991). Biosiliceous Particle Flux in the Southern Ocean. *Mar. Chem.* 35, 503–536. doi:10.1016/s0304-4203(09)90040-8

Abrantes, F., Gil, I., Lopes, C., and Castro, M. (2005). Quantitative Diatom Analyses-A Faster Cleaning Procedure. *Deep Sea Res. Oceanographic Res. Pap.* 52, 189–198. doi:10.1016/j.dsr.2004.05.012

Alldredge, A., and Gotschalk, C. (1989). Direct Observations of the Mass Flocculation of Diatomblooms - Characteristics, Settling Velocities and Formation of Diatom Aggregates. *Deep- Sea Res.* 36 (2), 159–171 .

Alley, K., Patacca, K., Pike, J., Dunbar, R., and Leventer, A. (2018). Iceberg Alley, East Antarctic Margin: Continuously Laminated Diatomaceous Sediments from the Late Holocene. *Mar. Micropaleontology* 140, 56–68. doi:10.1016/j.marmicro.2017.12.002

Annett, A. L., Carson, D. S., Crosta, X., Clarke, A., and Ganeshram, R. S. (2010). Seasonal Progression of Diatom Assemblages in Surface Waters of Ryder Bay, Antarctica. *Polar Biol.* 33 (1), 13–29. doi:10.1007/s00300-009-0681-7

Ardelan, M. V., Holm-Hansen, O., Hewes, C. D., Reiss, C. S., Silva, N. S., Dulaiova, H., et al. (2010). Natural Iron Enrichment Around the Antarctic Peninsula in the Southern Ocean. *Biogeosciences* 7, 11–25. doi:10.5194/bg-7-11-2010

Armand, L. K., Crosta, X., Romero, O., and Pichon, J.-J. (2005). The Biogeography of Major Diatom Taxa in Southern Ocean Sediments. *Palaeogeogr. Palaeoclimatol. Palaeoecol.* 223, 93–126. doi:10.1016/j.palaeo.2005.02.015

Arrigo, K. R., Robinson, D. H., Worthen, D. L., Dunbar, R. B., DiTullio, G. R., VanWoert, M., et al. (1999). Phytoplankton Community Structure and the Drawdown of Nutrients and CO2 in the Southern Ocean. *Science* 283, 365–367. doi:10.1126/science.283.5400.365

Assmy, P., Smetacek, V., Montresor, M., Klaas, C., Henjes, J., Strass, V. H., et al. (2013). Thick-shelled, Grazer-Protected Diatoms Decouple Ocean Carbon and Silicon Cycles in the Iron-Limited Antarctic Circumpolar Current. *Proc. Natl. Acad. Sci. U.S.A.* 110, 633–638. doi:10.1073/pnas.1309345110

Bathmann, U., Fisher, G., Müller, P. J., and Gerdes, D. (1991). Short-term Variations in Particulate Matter Sedimentation off Kapp Norvegia, Weddell Sea, Antarctica: Relation to Water Mass Advection, Ice Cover, Plankton Biomass and Feeding Activity. *Polar Biol.* 11, 185–195. doi:10.1007/bf00240207

Bathmann, U. V., Scharek, R., Klaas, C., Dubischar, C. D., and Smetacek, V. (1997). Spring Development of Phytoplankton Biomass and Composition in Major Water Masses of the Atlantic Sector of the Southern Ocean. *Deep Sea Res. Part Topical Stud. Oceanography* 44, 51–67. doi:10.1016/s0967-0645(96)00063-x

Battarbee, R. W. (1973). A New Method for the Estimation of Absolute Microfossil Numbers, with Reference Especially to Diatoms. *Limnol. Oceanogr.* 18, 647–653. doi:10.4319/lo.1973.18.4.0647

Berg, G. M., Mills, M. M., Long, M. C., Bellerby, R., Strass, V., Savoye, N., et al. (2011). Variation in Particulate C and N Isotope Composition Following Iron Fertilization in Two Successive Phytoplankton Communities in the Southern Ocean. *Glob. Biogeochem. Cycles* 25, a–n. doi:10.1029/2010gb003824

Bodungen, B. v., Smetacek, V. S., Tilzer, M. M., and Zeitzschel, B. (1986). Primary Production and Sedimentation during spring in the Antarctic Peninsula Region. *Deep Sea Res. A. Oceanographic Res. Pap.* 33, 177–194. doi:10.1016/0198-0149(86)90117-2

Boetius, A., Albrecht, S., Bakker, K., Bienhold, C., Felden, J., Fernandez-Mendez, M., et al. (2013). Export of Algal Biomass from the Melting Arctic Sea Ice. *Science*, 339, 1430–1432. doi:10.1126/science.1231346

Boyd, P. W. (2013). Diatom Traits Regulate Southern Ocean Silica Leakage. *Proc. Nat. Acad. Sci. U.S.A.* 110 (20), 358–359.,

Boyd, P. W., Dillingham, P. W., McGraw, C. M., Armstrong, E. A., Cornwall, C. E., Feng, Y.-y., et al. (2016). Physiological Responses of a Southern Ocean Diatom to Complex Future Ocean Conditions. *Nat. Clim Change* 6, 207–213. doi:10.1038/nclimate2811

Boyd, P. W., Jickells, T., Law, C. S., Blain, S., Boyle, E. A., Buesseler, K. O., et al. (2007). Mesoscale Iron Enrichment Experiments 1993-2005: Synthesis and Future Directions. *Science* 315, 612–617. doi:10.1126/science.1131669

Brix, H., Menemenlis, D., Hill, C., Dutkiewicz, S., Jahn, O., Wang, D., et al. (2015). Using Green's Functions to Initialize and Adjust a Global, Eddying Ocean Biogeochemistry General Circulation Model. *Ocean Model.* 95, 1–14. doi:10.1016/j.ocemod.2015.07.008

Brzezinski, M. A., Pride, C. J., Franck, V. M., Sigman, D. M., Sarmiento, J. L., Matsumoto, K., et al. (2002). A Switch from Si(OH)4to NO3−depletion in the Glacial Southern Ocean. *Geophys. Res. Lett.* 29 (12), 5-1–5-4. doi:10.1029/2001GL014349

Buma, A. G. J., de Baar, H. J. W., Nolting, R. F., and van Bennekom, A. J. (1991). Metal Enrichment Experiments in the Weddell-Scotia Seas: Effects of Iron and Manganese on Various Plankton Communities. *Limnol. Oceanogr.* 36 (8), 1865–1878. doi:10.4319/lo.1991.36.8.1865

Carroll, D., Menemenlis, J. F., Bowman, K. W., Brix, H., Dutkiewicz, S., et al. (2020). Seasonal to Multi-Decadal Air-Sea CO_2 Fluxes from the Data-Constrained ECCO-Darwin Global Ocean Biogeochemistry Model. *J. Adv. Model. Earth Sy.* 12, e2019MS001888. doi:10.1029/2019ms001888

Cavalieri, D., Parkinson, C., Gloersen, P., and Zwally, H. (2016). *Sea Ice Concentrations from Nimbus-7 SMMR and DMSP SSM/I-SSMIS Passive Microwave Data, Version 1. Boulder*, Colorado USA. NASA National Snow and Ice Data Center Distributed Active Archive Center. 1996, updated yearly). doi:10.5067/8GQ8LZQVL0VL

Crawford, R. M. (1995). The Role of Sex in the Sedimentation of a marine Diatom Bloom. *Limnol. Oceanogr.* 40 (1), 200–204. doi:10.4319/lo.1995.40.1.0200

de Baar, H. J. W., de Jong, J. T. M., Bakker, D. C. E., Loscher, B. M., Veth, C., Bathmann, U., et al. (1995). Importance of Iron for Plankton Blooms and Carbon Dioxide Drawdown in the Southern Ocean. *Nature* 373, 6513. doi:10.1038/373412a0

de Jong, J., Schoemann, V., Lannuzel, D., Croot, P., de Baar, H., and Tison, J.-L. (2012). Natural Iron Fertilization of the Atlantic Sector of the Southern Ocean by continental Shelf Sources of the Antarctic Peninsula. *J. Geophys. Res.* 117, G01029. doi:10.1029/2011JG001679

DeMaster, D. J. (2002). The Accumulation and Cycling of Biogenic Silica in the Southern Ocean: Revisiting the marine Silica Budget. *Deep Sea Res. Part Topical Stud. Oceanography* 49, 3155–3167. doi:10.1016/s0967-0645(02)00076-0

Dulaiova, H., Ardelan, M. V., Henderson, P. B., and Charette, M. A. (2009). Shelf-derived Iron Inputs Drive Biological Productivity in the Southern Drake Passage. *Glob. Biogeochem. Cycles* 23, a–n. doi:10.1029/2008GB003406

Dutkiewicz, S., Hickman, A. E., Jahn, O., Gregg, W. W., Mouw, C. B., and Follows, M. J. (2015). Capturing Optically Important Constituents and Properties in a

marine Biogeochemical and Ecosystem Model. *Biogeosciences* 12 (14), 4447–4481. doi:10.5194/bg-12-4447-2015

Dutkiewicz, S., Hickman, A. E., Jahn, O., Henson, S., Beaulieu, C., and Monier, E. (2019). Ocean Colour Signature of Climate Change. *Nat. Commun* 10 (1), 578. doi:10.1038/s41467-019-08457-x

Falkowski, P. G., Barber, R., and Smetacek, V. (1998). Biogeochemical Controls and Feedbacks on Ocean Primary Production. *Science* 281, 200–206. doi:10.1126/science.281.5374.200

Fischer, G., Gersonde, R., and Wefer, G. (2002). Organic Carbon, Biogenic Silica and Diatom Fluxes in the Marginal winter Sea-Ice Zone and in the Polar Front Region: Interannual Variations and Differences in Composition. *Deep Sea Res. Part Topical Stud. Oceanography* 49, 1721–1745. doi:10.1016/s0967-0645(02)00009-7

Fisher, G., and Karakaç, G. (2009). Sinking Rates and Ballast Composition of Particles in the Atlantic Ocean: Implications for the Organic Carbon Fluxes to the Deep Ocean. *Biogeosciences* 6, 85–102. doi:10.5194/bg-6-85-2009

Flexas, M. M., Schodlok, M. P., Padman, L., Menemenlis, D., and Orsi, A. H. (2015). Role of Tides on the Formation of the Antarctic Slope Front at the Weddell-Scotia Confluence. *J. Geophys. Res. Oceans* 120, 3658–3680. doi:10.1002/2014jc010372

Follows, M. J., Dutkiewicz, S., Grant, S., and Chisholm, S. W. (2007). Emergent Biogeography of Microbial Communities in a Model Ocean. *Science* 315, 1843–1846. doi:10.1126/science.1138544

Follows, M. J., and Dutkiewicz, S. (2011). Modeling Diverse Communities of marine Microbes. *Annu. Rev. Mar. Sci.* 3 (1), 427–451. doi:10.1146/annurev-marine-120709-142848

Froneman, P. W., Pakhomov, E. A., and Laubscher, R. K. (1997). Microphytoplankton Assemblages in the Waters Surrounding South Georgia, Antarctica during Austral Summer 1994. *Polar Biol.* 17, 515–522. doi:10.1007/s003000050150

Froneman, P. W., Perissinotto, R., McQuaid, C. D., and Laubscher, R. K. (1995). Summer Distribution of Netphytoplankton in the Atlantic Sector of the Southern Ocean. *Polar Biol.* 15, 77–84. doi:10.1007/bf00241045

Fryxell, G. (1989). Marine Phytoplankton at the Weddell Sea Ice Edge: Seasonal Changes at the Specific Level. *Polar Biol.* 10, 1–18. doi:10.1007/bf00238285

Gersonde, R., and Wefer, G. (1987). Sedimentation of Biogenic Siliceous Particles in Antarctic Waters from the Atlantic Sector. *Mar. Micropaleontology* 11, 311–332. doi:10.1016/0377-8398(87)90004-1

Grigorov, I., Rigual-Hernandez, A. S., Honjo, S., Kemp, A. E. S., and Armand, L. K. (2014). Settling Fluxes of Diatoms to the interior of the Antarctic Circumpolar Current along 170°W. *Deep Sea Res. Part Oceanographic Res. Pap.* 93, 1–13. doi:10.1016/j.dsr.2014.07.008

Hamm, C. E., Merkel, R., Springer, O., Jurkojc, P., Maier, C., Prechtel, K., et al. (2003). Architecture and Material Properties of Diatom Shells Provide Effective Mechanical protection. *Nature* 421, 841–843. doi:10.1038/nature01416

Hatta, M., Measures, C. I., Selph, K. E., Zhou, M., and Hiscock, W. T. (2013). Iron Fluxes from the Shelf Regions Near the South Shetland Islands in the Drake Passage during the Austral-winter 2006. *Deep Sea Res. Part Topical Stud. Oceanography* 90, 89–101. doi:10.1016/j.dsr2.2012.11.003

Henley, S. F., Annett, A. L., Ganeshram, R. S., Carson, D. S., Weston, K., Crosta, X., et al. (2012). Factors Influencing the Stable Carbon Isotopic Composition of Suspended and Sinking Organic Matter in the Coastal Antarctic Sea Ice Environment. *Biogeosciences* 9, 1137–1157. doi:10.5194/bg-9-1137-2012

Heussner, S., Ratti, C., and Carbonne, J. (1990). The PPS 3 Time-Series Sediment Trap and the Trap Sample Processing Techniques Used during the ECOMARGE experiment. *Continental Shelf Res.* 10, 943–958. doi:10.1016/0278-4343(90)90069-x

Heywood, K. J., Naveira Garabato, A. C., Stevens, D. P., and Muench, R. D. (2004). On the Fate of the Antarctic Slope Front and the Origin of the Weddell Front. *J. Geophys. Res.* 109, C06021. doi:10.1029/2003JC002053

Hoffmann, L., Peeken, I., Lochte, K., Assmy, P., and Veldhuis, M. (2006). Different Reactions of Southern Ocean Phytoplankton Size Classes to Iron Fertilization. *Limnol. Oceanogr.* 51 (3), 4231217–4231229. doi:10.4319/lo.2006.51.3.1217

Holland, P. R., and Kwok, R. (2012). Wind-driven Trends in Antarctic Sea-Ice Drift. *Nat. Geosci* 5, 872–875. doi:10.1038/ngeo1627

Holmhansen, O., Naganobu, M., Kawaguchi, S., Kameda, T., Krasovski, I., Tchernyshkov, P., et al. (2004). Factors Influencing the Distribution, Biomass, and Productivity of Phytoplankton in the Scotia Sea and Adjoining Waters. *Deep Sea Res. Part Topical Stud. Oceanography* 51, 1333–1350. doi:10.1016/s0967-0645(04)00083-9

Honjo, S. (2004). Particle export and the Biological Pump in the Southern Ocean. *Antarct. Sci.* 16, 430–501. doi:10.1017/s0954102004002287

Hutchins, D. A., and Bruland, K. W. (1998). Iron-limited Diatom Growth and Si:N Uptake Ratios in a Coastal Upwelling Regime. *Nature* 393, 561–564. doi:10.1038/31203

Ichinomiya, M., Gomi, Y., Nakamachi, M., Honda, M., Fukuchi, M., and Taniguchi, A. (2008). Temporal Variations in the Abundance and Sinking Flux of Diatoms under Fast Ice in Summer Near Syowa Station, East Antarctica. *Polar Sci.* 2, 33–40. doi:10.1016/j.polar.2008.01.001

Jacobs, S. S. (1991). On the Nature and Significance of the Antarctic Slope Front. *Mar. Chem.* 35, 9–24. doi:10.1016/s0304-4203(09)90005-6

Jiang, M., Measures, C. I., Barbeau, K. A., Charette, M. A., Gille, S. T., Hatta, M., et al. (2019). Fe Sources and Transport from the Antarctic Peninsula Shelf to the Southern Scotia Sea. *Deep Sea Res. Part Oceanographic Res. Pap.* 150, 103060. doi:10.1016/j.dsr.2019.06.006

Jordan, R. W., Priddle, J., Pudsey, C. J., Barker, P. F., and Whitehouse, M. J. (1991). Unusual Diatom Layers in Upper Pleistocene Sediments from the Northern Weddell Sea. *Deep Sea Res. Part A. Oceanographic Res. Pap.* 38 (7), 829–843. doi:10.1016/0198-0149(91)90021-7

Kamatani, A., and Oku, O. (2000). Measuring Biogenic Silica in marine Sediments. *Mar. Chem.* 68 (3), 219–229. doi:10.1016/s0304-4203(99)00079-1

Kemp, A. E. S., Pearce, R. B., Grigorov, I., Rance, J., Lange, C. B., Quilty, P., et al. (2006). Production of Giant marine Diatoms and Their export at Oceanic Frontal Zones: Implications for Si and C Flux from Stratified Oceans. *Glob. Biogeochem. Cycles* 20, a–n. doi:10.1029/2006GB002698

Kinney, J. C., Maslowski, W., Osinski, R., Jin, M., Frants, M., Jeffery, N., et al. (2020). Hidden Production: On the Importance of Pelagic Phytoplankton Blooms beneath Arctic Sea Ice. *J. Geophys. Res. Oceans* 125, e2020JC016211. doi:10.1029/2020JC016211

Klunder, M. B., Laan, P., De Baar, H. J. W., Middag, R., Neven, I., and Van Ooijen, J. (2014). Dissolved Fe across the Weddell Sea and Drake Passage: Impact of DFe on Nutrient Uptake. *Biogeosciences* 11, 651–669. doi:10.5194/bg-11-651-2014

Korb, R. E., Whitehouse, M. J., Thorpe, S. E., and Gordon, M. (2005). Primary Production across the Scotia Sea in Relation to the Physico-Chemical Environment. *J. Mar. Syst.* 57, 231–249. doi:10.1016/j.jmarsys.2005.04.009

Krause, J. W., and Lomas, M. W. (2020). Understanding Diatoms' Past and Future Biogeochemical Role in High-Latitude Seas. *Geophys. Res. Lett.* 47, e2019GL085602. doi:10.1029/2019GL085602

Landry, M. R., Selph, K. E., Brown, S. L., Abbott, M. R., Measures, C. I., Vink, S., et al. (2002). Seasonal Dynamics of Phytoplankton in the Antarctic Polar Front Region at 170°W. *Deep Sea Res. Part Topical Stud. Oceanography* 49, 1843–1865. doi:10.1016/s0967-0645(02)00015-2

Lannuzel, D., Chever, F., van der Merwe, P. C., Janssens, J., Roukaerts, A., Cavagna, A.-J., et al. (2016). Iron Biogeochemistry in Antarctic Pack Ice during SIPEX-2. *Deep Sea Res. Part Topical Stud. Oceanography* 131, 111–122. doi:10.1016/j.dsr2.2014.12.003

Laubscher, R. K., Perissinotto, R., and McQuaid, C. D. (1993). Phytoplankton Production and Biomass at Frontal Zones in the Atlantic Sector of the Southern Ocean. *Polar Biol.* 13, 471–481. doi:10.1007/bf00233138

Legendre, P., and Gallagher, E. D. (2001). Ecologically Meaningful Transformations for Ordination of Species Data. *Oecologia* 129, 271–280. doi:10.1007/s004420100716

Leventer, A., Domack, E., Barkoukis, A., McAndrews, B., and Murray, J. (2002). Laminations from the Palmer Deep: A Diatom-Based Interpretation. *Paleoceanography* 17, 3–1. doi:10.1029/2001PA000624

Leventer, A., Dunbar, R. B., and DeMaster, D. J. (1993). Diatom Evidence for Late Holocene Climatic Events in Granite Harbor, Antarctica. *Paleoceanography* 8 (3), 373–386. doi:10.1029/93pa00561

Leventer, A. (1991). Sediment Trap Diatom Assemblages from the Northern Antarctic Peninsula Region. *Deep Sea Res. Part A. Oceanographic Res. Pap.* 38, 1127–1143. doi:10.1016/0198-0149(91)90099-2

Lundholm, N., and Hasle, G. R. (2008). Are Fragilariopsis Cylindrus and Fragilariopsis Nana Bipolar Diatoms? - Morphological and Molecular Analyses of Two Sympatic Species. *Nova Hedwigia* 133, 231–250 .

Maddison, E. J., Pike, J., and Dunbar, R. (2012). Seasonally Laminated Diatom-Rich Sediments from Dumont d'Urville Trough, East Antarctic Margin: Late-

Holocene Neoglacial Sea-Ice Conditions. *The Holocene* 22 (8), 857–875. doi:10.1177/0959683611434223

Manizza, M., Menemenlis, D., Zhang, H., and Miller, C. E. (2019). Modeling the Recent Changes in the Arctic Ocean CO 2 Sink (2006-2013). *Glob. Biogeochem. Cycles* 33, 420–438. doi:10.1029/2018gb006070

Manno, C., Stowasser, G., Enderlein, P., Fielding, S., and Tarling, G. A. (2015). The Contribution of Zooplankton Faecal Pellets to Deep-Carbon Transport in the Scotia Sea (Southern Ocean). *Biogeosciences* 12, 1955–1965. doi:10.5194/bg-12-1955-2015

Marchetti, A., and Cassar, N. (2009). Diatom Elemental and Morphological Changes in Response to Iron Limitation: a Brief Review with Potential Paleoceanographic Applications. *Geobiology* 7 (4), 419–431. doi:10.1111/j.1472-4669.2009.00207.x

Marshall, J., Adcroft, A., Hill, C., Perelman, L., and Heisey, C. (1997). A Finite-Volume, Incompressible Navier Stokes Model for Studies of the Ocean on Parallel Computers. *J. Geophys. Res.* 102, 5753–5766. doi:10.1029/96jc02775

Martin, J. H., Gordon, R. M., and Fitzwater, S. E. (1990). Iron in Antarctic Waters. *Nature* 345, 156–158. doi:10.1038/345156a0

Matsumoto, K., SarmientoBrzezinski, J. L. M. A., and Brzezinski, M. A. (2002). Silicic Acid Leakage from the Southern Ocean: A Possible Explanation for Glacial atmosphericpCO2. *Glob. Biogeochem. Cycles* 16, 5–1. doi:10.1029/2001GB001442

Measures, C. I., Brown, M. T., Selph, K. E., Apprill, A., Zhou, M., Hatta, M., et al. (2013). The Influence of Shelf Processes in Delivering Dissolved Iron to the HNLC Waters of the Drake Passage, Antarctica. *Deep Sea Res. Part Topical Stud. Oceanography* 90, 77–88. doi:10.1016/j.dsr2.2012.11.004

Monien, D., Monien, P., Brünjes, R., Widmer, T., Kappenberg, A., Silva Busso, A. A., et al. (2017). Meltwater as a Source of Potentially Bioavailable Iron to Antarctica Waters. *Antarctic Sci.* 29, 277–291. doi:10.1017/S095410201600064X

Moore, J., and Villareal, T. (1996). Buoyancy and Growth Characteristics of Three Positively Buoyant marine Diatoms. *Mar. Ecol. Prog. Ser.* 132 (1–3), 203–213. doi:10.3354/meps132203

Mortlock, R. A., and Froelich, P. N. (1989). A Simple Method for the Rapid Determination of Biogenic Opal in Pelagic marine Sediments. *Deep Sea Res. Part A. Oceanographic Res. Pap.* 36, 1415–1426. doi:10.1016/0198-0149(89)90092-7

Naveira Garabato, A. C., Heywood, K. J., and Stevens, D. P. (2002). Modification and Pathways of Southern Ocean Deep Waters in the Scotia Sea. *Deep Sea Res. Part Oceanographic Res. Pap.* 49, 681–705. doi:10.1016/s0967-0637(01)00071-1

Nelson, D. M., and Gordon, L. I. (1982). Production and Pelagic Dissolution of Biogenic Silica in the Southern Ocean. *Geochimica et Cosmochimica Acta* 46, 491–501. doi:10.1016/0016-7037(82)90153-3

Nunes, S., Latasa, M., Delgado, M., Emelianov, M., Simó, R., and Estrada, M. (2019). Phytoplankton Community Structure in Contrasting Ecosystems of the Southern Ocean: South Georgia, South Orkneys and Western Antarctic Peninsula. *Deep Sea Res. Part Oceanographic Res. Pap.* 151, 103059. doi:10.1016/j.dsr.2019.06.005

Oksanen, J., Blanchet, F. G., Friendly, M., Kindt, R., Legendre, P., McGlinn, D., et al. (2015). Vegan: Community Ecology. Avaliable at: http://CRAN.R-project.org/package=vegan (Accessed March 20, 2016).

Orsi, A. H., Nowlin, W. D., Jr., and Whitworth, T., III (1993). On the Circulation and Stratification of the Weddell Gyre. *Deep Sea Res. Part Oceanographic Res. Pap.* 40, 169–203. doi:10.1016/0967-0637(93)90060-g

Orsi, A. H., Whitworth, T., III, and Nowlin, W. D., Jr (1995). On the Meridional Extent and Fronts of the Antarctic Circumpolar Current. *Deep Sea Res. Part Oceanographic Res. Pap.* 42, 641–673. doi:10.1016/0967-0637(95)00021-w

Palmer, M., Gomis, D., Flexas, M. d. M., Jordà, G., Jullion, L., Tsubouchi, T., et al. (2012). Water Mass Pathways and Transports over the South Scotia Ridge West of 50°W. *Deep Sea Res. Part Oceanographic Res. Pap.* 59, 8–24. doi:10.1016/j.dsr.2011.10.005

Patterson, S. L., and Sievers, H. A. (1980). The Weddell-Scotia Confluence. *J. Phys. Oceanogr.* 10, 1584–1610. doi:10.1175/1520-0485(1980)010<1584:twsc>2.0.co;2

Peloquin, J. A., and Smith, W. O., Jr (2006). The Role of Phytoplankton Size on Photochemical Recovery during the Southern Ocean Iron experiment. *J. Phycol.* 42, 1016–1027. doi:10.1111/j.1529-8817.2006.00266.x

Pilskaln, C. H., Manganini, S. J., Trull, T. W., Armand, L., Howard, W., Asper, V. L., et al. (2004). Geochemical Particle Fluxes in the Southern Indian Ocean Seasonal Ice Zone: Prydz Bay Region, East Antarctica. *Deep Sea Res. Part Oceanographic Res. Pap.* 51, 307–332. doi:10.1016/j.dsr.2003.10.010

Pondaven, P., Ragueneau, O., Tréguer, P., Hauvespre, A., Dezileau, L., and Reyss, J. L. (2000). Resolving the 'opal Paradox' in the Southern Ocean. *Nature* 405, 168–172. doi:10.1038/35012046

Quéguiner, B. (2013). Iron Fertilization and the Structure of Planktonic Communities in High Nutrient Regions of the Southern Ocean. *Deep Sea Res. Part Topical Stud. Oceanography* 90, 43–54. doi:10.1016/j.dsr2.2012.07.024

Ragueneau, O., Tréguer, p., Leynaert, A., Anderson, R. F., Brzezinski, M. A., DeMaster, D. J., et al. (2000). A Review of the Si Cycle in the Modern Ocean: Recent Progress and Missing Gaps in the Application of Biogenic Opal as a Paleoproductivity Proxy. *Glob. Planet. Change* 26, 317–365. doi:10.1016/s0921-8181(00)00052-7

Rembauville, M., Blain, S., Blain, S., Armand, L., Quéguiner, B., and Salter, I. (2015). Export Fluxes in a Naturally Iron-Fertilized Area of the Southern Ocean - Part 2: Importance of Diatom Resting Spores and Faecal Pellets for export. *Biogeosciences* 12, 3171–3195. doi:10.5194/bg-12-3171-2015

Rembauville, M., Manno, C., Tarling, G. A., Blain, S., and Salter, I. (2016). Strong Contribution of Diatom Resting Spores to Deep-Sea Carbon Transfer in Naturally Iron-Fertilized Waters Downstream of South Georgia. *Deep Sea Res. Part Oceanographic Res. Pap.* 115, 22–35. doi:10.1016/j.dsr.2016.05.002

Rembauville, M., Salter, I., Dehairs, F., Miquel, J.-C., and Blain, S. (2018). Annual Particulate Matter and Diatom export in a High Nutrient, Low Chlorophyll Area of the Southern Ocean. *Polar Biol.* 41, 25–40. doi:10.1007/s00300-017-2167-3

Rigual-Hernández, A. S., Pilskaln, C. H., Cortina, A., Abrantes, F., and Armand, L. K. (2019). Diatom Species Fluxes in the Seasonally Ice-Covered Antarctic Zone: New Data from Offshore Prydz Bay and Comparison with Other Regions from the Eastern Antarctic and Western Pacific Sectors of the Southern Ocean. *Deep Sea Res. Part Topical Stud. Oceanography* 161, 92–104. doi:10.1016/j.dsr2.2018.06.005

Rigual-Hernández, A. S., Trull, T. W., Bray, S. G., and Armand, L. K. (2016). The Fate of Diatom Valves in the Subantarctic and Polar Frontal Zones of the Southern Ocean: Sediment Trap versus Surface Sediment Assemblages. *Palaeogeogr. Palaeoclimatol. Palaeoecol.* 457, 129–143. doi:10.1016/j.palaeo.2016.06.004

Rigual-Hernández, A. S., Trull, T. W., Bray, S. G., Closset, I., and Armand, L. K. (2015). Seasonal Dynamics in Diatom and Particulate export Fluxes to the Deep Sea in the Australian Sector of the Southern Antarctic Zone. *J. Mar. Syst.* 142, 62–74. doi:10.1016/j.jmarsys.2014.10.002

Salter, I., Kemp, A. E. S., Moore, C. M., Lampitt, R. S., Wolff, G. A., and Holtvoeth, J. (2012). Diatom Resting Spore Ecology Drives Enhanced Carbon export from a Naturally Iron-Fertilized Bloom in the Southern Ocean. *Glob. Biogeochem. Cycles* 26, a–n. doi:10.1029/2010GB003977

Salter, I., Lampitt, R. S., Sanders, R., Poulton, A., Kemp, A. E. S., Boorman, B., et al. (2007). Estimating Carbon, Silica and Diatom export from a Naturally Fertilised Phytoplankton Bloom in the Southern Ocean Using PELAGRA: A Novel Drifting Sediment Trap. *Deep Sea Res. Part Topical Stud. Oceanography* 54, 2233–2259. doi:10.1016/j.dsr2.2007.06.008

Sanchez, N., Reiss, C. S., Holm-Hansen, O., Hewes, C. D., Bizsel, K. C., and Ardelan, M. V. (2019). Weddell-Scotia confluence Effect on the Iron Distribution in Waters Surrounding the South Shetland (Antarctic Peninsula) and South Orkney (Scotia Sea) Islands during the Austral Summer in 2007 and 2008. *Front. Mar. Sci.* 6, 771. doi:10.3389/fmars.2019.00771

Sarmiento, J. L., Gruber, N., Brzezinski, M. A., and Dunne, J. P. (2004). High-latitude Controls of Thermocline Nutrients and Low Latitude Biological Productivity. *Nature* 427, 56–60. doi:10.1038/nature02127

Sedwick, P. N., Harris, P. T., Robertson, L. G., McMurtry, G. M., Cremer, M. D., and Robinson, P. (2001). Holocene Sediment Records from the continental Shelf of Mac. Robertson Land, East Antarctica. *Paleoceanography* 16 (2), 212–225. doi:10.1029/2000pa000504

Shen, C., Dupont, C. L., and Hopkinson, B. M. (2017). The Diversity of CO2-concentrating Mechanisms in marine Diatoms as Inferred from Their Genetic Content. *J. Exp. Bot.* 68, 3937–3948. doi:10.1093/jxb/erx163

Sigman, D. M., Altabet, M. A., McCorkle, D. C., Francois, R., and Fischer, G. (1999). The δ15N of Nitrate in the Southern Ocean: Consumption of Nitrate in

Surface Waters. *Glob. Biogeochem. Cycles* 13, 1149–1166. doi:10.1029/1999gb900038

Sigman, D. M., Altabet, M. A., McCorkle, D. C., Francois, R., and Fischer, G. (2000). The δ15N of Nitrate in the Southern Ocean: Nitrogen Cycling and Circulation in the Ocean interior. *J. Geophys. Res.* 105, 19599–19614. doi:10.1029/2000jc000265

Singler, H. R., and Villareal, T. A. (2005). Nitrogen Inputs into the Euphotic Zone by Vertically Migrating Rhizosolenia Mats. *J. Plankton Res.* 27, 545–556. doi:10.1093/plankt/fbi030

Smetacek, V., Assmy, P., and Henjes, J. (2004). The Role of Grazing in Structuring Southern Ocean Pelagic Ecosystems and Biogeochemical Cycles. *Antartic Sci.* 16 (4), 541–558. doi:10.1017/s0954102004002317

Smetacek, V., Klaas, C., Menden-Deuer, S., and Rynearson, T. A. (2002). Mesoscale Distribution of Dominant Diatom Species Relative to the Hydrographical Field along the Antarctic Polar Front. *Deep Sea Res. Part Topical Stud. Oceanography* 49, 3835–3848. doi:10.1016/s0967-0645(02)00113-3

Smetacek, V., Klaas, C., Strass, V. H., Assmy, P., Montresor, M., Cisewski, B., et al. (2012). Deep Carbon export from a Southern Ocean Iron-Fertilized Diatom Bloom. *Nature* 487, 313–319. doi:10.1038/nature11229

Smetacek, V. S. (1985). Role of Sinking in Diatom Life-History Cycles: Ecological, Evolutionary and Geological Significance. *Mar. Biol.* 84, 239–251. doi:10.1007/bf00392493

Spreen, G., Kaleschke, L., and Heygster, G. (2008). Sea Ice Remote Sensing Using AMSR-E 89-GHz Channels. *J. Geophys. Res.* 113, C02S03. doi:10.1029/2005JC0033810.1029/2005jc003384

Takeda, S. (1998). Influence of Iron Availability on Nutrient Consumption Ratio of Diatoms in Oceanic Waters. *Nature* 393, 774–777. doi:10.1038/31674

Taylor, F., and Sjunneskog, C. (2002). Postglacial marine Diatom Record of the Palmer Deep, Antarctic Peninsula (ODP Leg 178, Site 1098) 2. Diatom Assemblages. *Paleoceanography* 17 (3), 2–1. doi:10.1029/2000pa000564

ter Braak, C. J. F. (1986). Canonical Correspondence Analysis: a New Eigenvector Technique for Multivariate Direct Gradient Analysis. *Ecology* 67, 1167–1179. doi:10.2307/1938672

Thompson, A. F., and Youngs, M. K. (2013). Surface Exchange between the Weddell and Scotia Seas. *Geophys. Res. Lett.* 40, 5920–5925. doi:10.1002/2013gl058114

Timmermans, K. R., van der Wagt, B., and de Baar, H. J. W. (2004). Growth Rates, Half-Saturation Constants, and Silicate, Nitrate, and Phosphate Depletion in Relation to Iron Availability of Four Large, Open-Ocean Diatoms from the Southern Ocean. *Limnol. Oceanogr.* 49, 2141–2151. doi:10.4319/lo.2004.49.6.2141

Tréguer, P., Bowler, C., Moriceau, B., Dutkiewicz, S., Gehlen, M., Aumont, O., et al. (2017). Influence of Diatom Diversity on the Ocean Biological Carbon Pump. *Nat. Geosci* 11, 27–37. doi:10.1038/s41561-017-0028-x

Tschudi, M., Fowler, C., Maslanik, J., Stewart, J. S., and Meier, W. (2016). *Polar Pathfinder Daily 25 Km EASE-Grid Sea Ice Motion Vectors, Version 3. Boulder*, Colorado USA. NASA National Snow and Ice Data Center Distributed Active Archive Center. doi:10.5067/O57VAIT2AYYY

Villareal, T. A., Altabet, M. A., and Culver-Rymsza, K. (1993). Nitrogen Transport by Vertically Migrating Diatom Mats in the north Pacific Ocean. *Nature* 363, 709–712. doi:10.1038/363709a0

Villareal, T. A., Joseph, L., Brzezinski, M. A., Shipe, R. F., Lipschultz, F., and Altabet, M. A. (1999b). Biological and Chemical Characteristics of the Giant Diatom Ethmodiscus (Bacillariophyceae) in the central North Pacific Gyre. *J. Phycol.* 35, 896–902. doi:10.1046/j.1529-8817.1999.3550896.x

Villareal, T. A., Pilskaln, C., Brzezinski, M., Lipschultz, F., Dennett, M., and Gardner, G. B. (1999a). Upward Transport of Oceanic Nitrate by Migrating Diatom Mats. *Nature* 397, 423–425. doi:10.1038/17103

Wang, S., Bailey, D., Lindsay, K., Moore, J. K., and Holland, M. (2014). Impact of Sea Ice on the marine Iron Cycle and Phytoplankton Productivity. *Biogeosciences* 11, 4713–4731. doi:10.5194/bg-11-4713-2014

Whitehouse, M. J., Korb, R. E., A., A., Atkinson, S. E., and Gordon, M. (2008). Formation, Transport and Decay of an Intense Phytoplankton Bloom within the High-Nutrient Low-Chlorophyll belt of the Southern Ocean. *J. Mar. Syst.* 70, 150–167. doi:10.1016/j.jmarsys.2007.05.003

Whitworth, T., III, Nowlin, W. D., Jr., Orsi, A. H., Locarnini, R. A., and Smith, S. G. (1994). Weddell Sea Shelf Water in the Bransfield Strait and Weddell-Scotia Confluence. *Deep Sea Res. Part Oceanographic Res. Pap.* 41, 629–641. doi:10.1016/0967-0637(94)90046-9

Wunsch, C., Heimbach, P., Ponte, R., and Fukumori, I. (2009). The Global General Circulation of the Ocean Estimated by the ECCO-Consortium. *Oceanog.* 22, 88–103. doi:10.5670/oceanog.2009.41

Youngs, M. K., Thompson, A. F., Flexas, M. M., and Heywood, K. J. (2015). Weddell Sea export Pathways from Surface Drifters. *J. Phys. Oc.* 45, 1068–1085. doi:10.1175/jpo-d-14-0103.1

Zhang, H., Menemenlis, D., and Fenty, I. G. (2018). ECCO LLC270 Ocean-Ice State Estimate. Available at: http://hdl.handle.net/1721.1/119821 (Accessed October 14, 2020).

Conflict of Interest: The authors declare that the research was conducted in the absence of any commercial or financial relationships that could be construed as a potential conflict of interest.